HHS Public Access

Author manuscript

Pain. Author manuscript; available in PMC 2018 December 01.

Published in final edited form as:

Pain. 2017 December ; 158(12): 2396–2409. doi:10.1097/j.pain.0000000000001044.

Tumor necrosis factor alpha secreted from oral squamous cell carcinoma contributes to cancer pain and associated inflammation

Nicole N. Scheff[1], **Yi Ye**[1], **Aditi Bhattacharya**[1], **Justin MacRae**[2], **Dustin H. Hickman**[2], **Atul K. Sharma**[2], **John C. Dolan**[1], and **Brian L. Schmidt**[1,*]

[1]New York University, Bluestone Center for Clinical Research, New York, NY 10010

[2]New York University, College of Dentistry, New York, NY 10010

Keywords

Cancer pain; Inflammation; Tumor necrosis factor alpha; Oral squamous cell carcinoma

1. Introduction

The prevalence and intensity of oral squamous cell carcinoma (oSCC) pain is higher than all other cancers [55,67]. While the etiology of cancer pain remains unknown, an often-cited hypothesis for cancer pain is that cancer cells and leukocytes within the cancer microenvironment produce mediators that sensitize and activate nociceptors [58]. Despite the strong inflammatory response that characterizes oral cancers, the role of leukocyte infiltration and associated secretion of mediators in oral cancer pain is unknown.

Immunotherapy is the most promising new anti-cancer approach; these drugs act on the programmed cell death (PD-1/PD-L1) protein axis. This therapeutic tactic has shown promise for oral cancers [9,41,79]. Inhibition of the PD-1/PD-L1 pathway using monoclonal antibodies enhances leukocyte infiltration and increases tumor necrosis factor alpha (TNFα) secretion into the oral cancer microenvironment [42]. TNFα is a pro-inflammatory cytokine implicated in nociceptive signaling. TNFα stimulation of nerve endings alters neuronal excitability [35,56] and produces heat hyperalgesia [12] and mechanical allodynia [44,69]. The emergence of the PD-1/PD-L1 pro-inflammatory drugs raises questions regarding the role of infiltrating leukocytes and TNFα in oral cancer pain and whether these drugs will exacerbate the significant pain associated with oral cancer.

The single study that has addressed the question of the role of inflammation in oral cancer pain used an orthotopic xenograft model in rats with Walker carcinomasarcoma 256B cells [28]. Carcinosarcoma is extremely rare in the oral cavity; squamous cell carcinoma is the most common oral cancer. Furthermore, orthotopic xenograft models do not reflect natural carcinogenesis [14,40]. To study the question of whether leukocyte infiltration and

*Corresponding Author: Brian L. Schmidt, Bluestone Center for Clinical Research, 2nd Floor, 421 1st Avenue, New York, NY 10010, 212-998-9543, brianl.schmidt@nyu.edu.

inflammatory mediators contributed to oral cancer pain, we compared the relationship of cancer-induced inflammation and nociception using two oral cancer pain mouse models: 1) a model of oral cancer pain created by injecting supernatant from human oral cancer cell lines into the tongue; and 2) a chronic carcinogen-induced cancer pain mouse model using 4-nitroquinoline-1-oxide (4NQO) [36,60]. Investigation of changes in the oral microenvironment, both in response to cancer-secreted mediators in the absence of tumor burden as well as during chemical-induced carcinogenesis with progressive stimulation of the immune system, aided in the disambiguation of the impact of inflammation on cancer-induced nociceptive behavior.

2. Methods

2.1 Cell Culture and Supernatant collection

Five cell lines were utilized to produce the acute supernatant cancer pain model and comparators: two oral cancer cell lines (HSC3 and SCC9), dysplastic cell line (DOK), melanoma cell line (SkMel28), and immortalized non-tumorigenic keratinocyte cell line (HaCaT). Cell lines were maintained and culture supernatant was collected as previously described [39,76]. All cell lines were cultured in 10 cm cell culture dishes at 37°C with 5% CO_2 in Dulbecco's modified Eagle's medium (DMEM, Gibco, Waltham, MA) supplemented with 10% fetal bovine serum and penicillin/streptomycin (50 U/mL). When cells reached 70–80% confluency (1.5×10^6 cells), the culture medium was changed to serum-free DMEM without phenol red (3 mL total volume), and incubated for 48 hours. Culture supernatant was then collected and frozen at −20°C until needed.

2.2 Animals

Adult (10–12 weeks, 20–30 g) female C57BL/6 mice (stock #000664, Jackson Labs, Bar Harbor, ME) and female NSG (NOD-*scid* IL2Rg^{null}, stock # 005557, Jackson Labs) mice were used for all experiments. All mice were housed in a temperature-controlled room on a 12:12 hour light cycle (0700–1900 hours light), with unrestricted access to food and water. All the procedures were approved by the New York University Committee on Animal Research. Researchers were trained under the Animal Welfare Assurance Program. All procedures were approved by the New York University Institutional Animal Care and Use Committee and performed in accordance with National Institutes of Health guidelines for the use of laboratory animals in research.

2.2.1 Acute supernatant oral cancer pain model—An acute supernatant oral cancer pain model was developed to quantify cancer-induced pain and inflammation by injecting cell line supernatant into the tongue. Mice received 50 μl injections of supernatant over a 5 second period, into the left lateral tongue under isoflurane general anesthesia for 3 consecutive days. TNFα-TNFR interaction modulator, C87 (5mM Stock in DMSO, EMD Millipore, Billerica, MA), was co-injected with supernatant for experiments designed to understand the role of TNFα in oral cancer pain and immune cell infiltration. Nociceptive behavior measurements using the dolognawmeter assay and device were recorded in awake mice at 1 hour after the third injection. Inflammatory infiltrate was measured using flow cytometry 12 hours after the third injection.

2.2.2 4NQO-induced oral cancer pain model—To study the development of oSCC including stages of early and late dysplasia, mice ingested the carcinogen 4-nitroquinoline-1-oxide (4NQO; 100 μg/ml; Sigma Aldrich, St. Louis, MO) with their drinking water on an unrestricted basis for 16 weeks. Water was changed weekly with freshly prepared 4NQO dissolved in propylene glycol (5 mg/ml) [66]. Control mice received water containing the equivalent dilution of propylene glycol alone. Functional allodynia, as a result of progressive 4NQO-induced carcinogenesis, was assessed using the dolognawmeter once a week for the full duration of the model (28 weeks). At the end of the experiment, tongue tissue was harvested, fixed in 10% buffered formalin, and processed for paraffin embedding and slide preparation. Tissue sections were cut at 4 μm and stained with hematoxylin & eosin (H & E) by the New York University Langone Medical Center Histopathology Core. A blinded oral pathologist at the New York University Bluestone Center for Clinical Research performed histopathological analyses to score dysplastic grade or determine the presence of oSCC.

2.3 Orofacial behavior

The dolognawmeter, a validated device and assay, was designed to measure oral function and nociception; the device and assay are validated for the measurement of functional nociception in mice with oral cancer [16]. Each mouse was placed into a confinement tube with 2 obstructing dowels in series; the mouse voluntarily gnaws through both dowels to escape the device. Each obstructing dowel is connected to a digital timer. The timer automatically stops when the mouse severs the dowel, recording the duration of time required to complete the behavior and escape the device. To acclimatize the mice and improve consistency in gnawing duration, all mice were trained for 5–7 sessions in the dolognawmeter. Training involves placing the animals in the device and allowing them to gnaw through the obstructing dowels in exactly the same manner that they do so during the subsequent experimental gnawing trials. For both oral cancer pain models, a baseline gnaw time to sever the second dowel was used as the mean of the final 3 training sessions for each mouse. The experimenter carrying out behavior assays was blinded to the treatment groups. Following the determination of baseline gnaw times, drug injections or 4NQO treatment was initiated and the mice underwent behavioral testing 1×/week for 28 weeks. Each mouse was normalized to its own baseline gnaw time and data is presented as a percent change ± standard error of the mean.

2.4 Isolation of tongue immune cells

Tongue tissue was dissected into cold DMEM containing antibiotics (penicillin/streptomycin, 10 U/mL) and 20 mM HEPES and dissociated per a protocol modified from that previously described [50]. Briefly, tongue tissue was dissected and minced in DMEM with antibiotics, collagenase-H (0.5 mg/ml; Sigma Aldrich, 34 Units/mg), DNase (0.5 mg/ml) and 20 mM HEPES, and then incubated at 37°C for 1 hour. The tissue was then mechanically dissociated using a fire-polished pipette, washed twice with fresh DMEM containing antibiotics and HEPES, and then resuspended in Ca^{2+}/Mg^{2+} free phosphate buffered saline (Sigma Aldrich) containing 3% fetal bovine serum, 1 mM EDTA, and 0.02% sodium azide and filtered through a 40 μm cell strainer (Falcon brand, Fisher Scientific, Waltham, MA).

2.4.1 Flow cytometry—Flow cytometry was used to characterize immune cell types within the mouse tongue. Within CD45+ hematopoietic cells, six subpopulations were detected and quantified using antibodies specific for receptors expressed on each cell type. Single-cell suspensions were prepared as described above and samples were stained with rat anti–mouse purified CD16/CD32 to block unspecific FC receptor binding. CD45 monoclonal antibody (mAb) conjugated with V450 dye (1:400; BD Biosciences Franklin Lakes, NJ) was used to label all hematopoietic cells. To differentiate leukocyte subpopulations, we stained cell suspensions with specific fluorescently conjugated rat anti-mouse mAbs recognizing neutrophils (Ly6G, 1:500), monocytes/macrophage/mast cells (CD11b, 1:1000), dendritic cells (CD11c, 1:250), T lymphocytes (CD3, 1:250), natural killer cells (NK1.1, 1:300), or B cells (CD49R, 1:500) (all BD Biosciences). The specificity of the staining was verified by incubation of cell suspensions with appropriate isotype-matched control antibodies. The gating strategy for isolation of these populations was to first to exclude dead cells (viability) in the population using propidium iodide (PI; Molecular Probes, Eugene, OR). Of the live cells recovered, CD45+ immune cells were first selected, and then sorted into CD11b+ macrophages/neutrophils/mast cells and CD11c+ dendritic cells. CD11b+/c− immune cells were further sorted into CD11b+/Ly6G+ and Ly6G− to isolate neutrophils. CD45+ cells were also sorted into CD3+ T-Cells and CD3- immune cells were further sorted into CD45R+ B-cells or NK1.1 natural killer cells. Viability was uniformly 70–85%, as determined by PI. This resulted in an average of $8.11 \times 10^5 \pm 4.1 \times 10^4$ live cells recovered per naïve tongue. Spleen cells were used for compensation controls. Data were acquired using a FACSCalibur (BD Biosciences) and analyzed using FlowJo software (Tree Star, San Carlos, CA).

2.5 Tongue primary afferent primary culture

2.5.1 Retrograde tracer labeling—At least 10 days prior to tissue harvest, the retrograde tracer 1,1′-dioctadecyl-3,3,3′,3′-tetramethy lindocarbocyanine perchlorate (DiI, Invitrogen, Carlsbad, CA) was injected peripherally into the anterior lateral portion of the tongue in order to label tongue afferents. For the 4NQO carcinogenesis model, mice were injected with DiI 10 days prior to the initiation of carcinogen treatment. The tracer was dissolved at 170 mg/ml in dimethylsufoxide (DMSO), diluted 1:10 in 0.9% sterile saline, and injected bilaterally using a 30 g needle for a total volume of 5–7 μL per tongue under isoflurane (Abbott Laboratories, North Chicago, IL) anesthesia.

2.5.2 Primary Culture—Adult female mice were anesthetized with isoflurane and transcardially perfused with cold Ca^{2+}/Mg^{2+}-free Hank's balanced salt solution (Invitrogen). Bilateral trigeminal ganglia (TG) were dissected into cold Hank's balanced salt solution and dissociated as previously described [46]. Cells were plated in Dulbecco modified Eagle medium F12 (Gibco) containing 5% fetal bovine serum and antibiotics (penicillin/streptomycin, 50 U/mL). Coverslips were flooded 2 h later with Leibovitz's L-15 media (Gibco) containing 10% FBS, 5 mM HEPES and 5 mM glucose, and used at room temperature. Experiments were performed within 8 hours of tissue harvest.

2.6 Patch Clamp Physiology

2.6.1 Current Clamp—Whole cell patch clamp recording was used to assess changes in the excitability of cultured retrogradely labeled TG neurons from naïve, vehicle-treated, and 4NQO-treated female C57BL/6 mice. Borosilicate glass electrodes were filled with 110 mM K-methanesulfonate, 30 mM KCl, 5 mM NaCl, 1 mM $CaCl_2$, 2 mM $MgCl_2$, 10 mM HEPES, 11 mM EGTA, 2 mM Mg-ATP, 1 mM Li-GTP, pH 7.2 (adjusted with Tris-base), 310 mOsm (adjusted with sucrose). Neurons were continuously superfused with a bath solution that contained 3 mM KCl, 130 mM NaCl, 2.5 mM $CaCl_2$, 0.6 mM $MgCl_2$, 10 mM HEPES, 10 mM glucose, pH 7.4 (adjusted with Tris-base), 325 mOsm (adjusted with sucrose). Cell line supernatants were applied with a computer-controlled perfusion fast-step system (switching time <20 ms; Warner Instrument Co, Hamden, CT, Model SF-77B). Oral cancer-induced changes in excitability were assessed in current-clamp mode by four distinct measures: spontaneous activity, action potential (AP) threshold, rheobase, and accommodation. Spontaneous activity was assessed at resting membrane potential (Vm) for 30 seconds at baseline and up to 90 seconds after the application of culture supernatant. The second two measures were determined with a 750 millisecond depolarizing square-pulse current injection. AP threshold was defined as the greatest depolarization reached before spike generation in response to depolarizing current injections. Rheobase was defined as the smallest amount of current needed to evoke a single AP. Because rheobase is positively correlated with cell size, values were normalized with respect to membrane capacitance to facilitate comparisons between neurons. Cancer supernatant-induced changes in accommodation (action potential generation) were assessed by a ramp and hold protocol consisting of a 250 millisecond ramp followed by 500 millisecond sustained current injection. Accommodation was determined by counting the number of action potentials (APs) evoked during this protocol. The magnitude of current injection was adjusted to evoke an AP during the ramp phase of the stimulation protocol. This protocol was then used to stimulate neurons every 30 seconds before and after application of cancer supernatant; at least three stimuli were used to establish the stability of neuronal excitability prior to the application of supernatant. Cancer supernatant was applied for approximately 3 minutes. There was no difference in baseline measurements between groups; therefore, to facilitate comparisons between neurons, supernatant-induced changes were analyzed as a percent change from baseline. Passive and active electrophysiological properties were also assessed. Passive properties assessed included Vm, capacitance and input resistance (R_{in}). R_{in} was measured with five 750 millisecond hyperpolarizing current injections (2–5 pA) from Vm. Active electrophysiological properties were assessed with an AP evoked by a 4 millisecond depolarizing current pulse. These included: AP duration at 0 mV, magnitude of AP overshoot, magnitude of the after-hyperpolarization (AHP), and AHP decay (τ AHP). The magnitude of the overshoot was measured from 0 mV. The magnitude of the AHP was measured from the Vm. Decay of the AHP was estimated by fitting the decay phase of the AHP with a single exponential function. Neurons with a cell body diameter greater than 10 μm and an inflection in the falling phase of the action potential were included in the study. For each afferent neuron isolated for study, a continuous recording was obtained for 60 seconds without the delivery of external stimulus. If spontaneous discharge persisted during this period, the neuron was classified as spontaneously active and disregarded.

2.7 Cytokine/chemokine protein quantification

Multiplex immunoassays were performed on 48 hour supernatants collected from three different passages of HSC3, SCC9, DOK, SkMel28, and HaCaT cell lines. Supernatants were analyzed using MILLIPLEX® MAP magnetic bead immunoassay kits (EMD Millipore) based on the Luminex® xMAP® technology. Protein biomarkers in supernatants were quantitatively determined using a MILLIPLEX® MAP Human Cytokine/Chemokine panel designed to detect 38 different cytokines/chemokines as per the manufacturer's instructions: EGF, FGF-2, Eotaxin, TGFα, G-CSF, Flt-3L, GM-CSF, Fractalkine, IFNα2, IFNγ, GRO, IL-10, MCP-3, IL-12p40, MDC, IL-12p70, IL-13, IL-15, sCD40L, IL-17A, IL-1RA, IL-1α, IL-9, IL-1b, IL-2, IL-3, IL-4, IL-5, IL-6, IL-7, IL-8, IP-10, MCP-1, MIP-1a, MIP-1b, TNFα, TNFβ, and VEGF. In brief, 25 μL of supernatant samples (or standards) were incubated with 25 μL of magnetic beads conjugated with capture antibodies in a 96-well plate overnight at 4°C. On day 2, the beads were washed, 25 or 50 μL biotinylated detection antibody cocktail was added and the assay plates were incubated at room temperature for 1 hour. Then, 25 μL streptavidin-phycoerythrin (SAPE) were added for an additional 30 minutes incubation. The beads were then washed and resuspended in 100 μL buffer to read on a Luminex® 200™ Instrument. The sample data were analyzed with the above listed proteins using MILLIPLEX® Analyst 5.1 software.

The TNFα concentration in tongue tissue from 4NQO-treated mice was measured by ELISA (MyBioSource, Inc; San Diego, CA). Frozen tissue (20–40 mg) was homogenized in the T-PER Reagent (Pierce Biotechnology, Inc., Rockford, IL) and agitated for an additional 2 hours at 4°C. The lysates were centrifuged at 13,000 rpm for 5 minutes. The supernatants were removed, aliquoted, and protein concentrations were determined using a Bradford Assay (Bio-Rad Laboratories, Inc., Hercules, CA). ELISA was run per the manufacturer's instructions. The optical density of the standards and samples was read at 450 nm using a Model 680 Microplate Reader (Bio-Rad Laboratories, Inc.).

2.8 Immunohistochemistry

Animals were euthanized via an overdose of inhaled isoflurane and perfused transcardially with 4% paraformaldehyde (PFA, Sigma Aldrich). TG were dissected, post-fixed for 1 hour in PFA and cryoprotected in 30% sucrose in 0.1M phosphate buffer (PB) at 4°C. TG were embedded in Tissue-Tek OCT compound (Sakura Finetek, Torrance, CA), sectioned (14 μm), and mounted on Superfrost Plus slides (Fisher Scientific Company, Pittsburgh, PA). After several washes, sections were incubated in primary antibody in PBS containing 1% BSA overnight at room temperature. The primary antibodies used were: isolectin B4 FITC conjugate (IB4-FITC (1:1000, Tocris, Bristol, UK), anti-CGRP (1:500, Abcam, Cambridge, UK), anti-NF200 (1:500, Abcam), anti-TNFR1 or TNFR2 (1:250, R&D Systems, Minneapolis, MN)). Slides were extensively washed in PBS and incubated in goat anti-rabbit secondary antibodies conjugated to cyanine 2 (Jackson ImmunoResearch, West Grove, PA) in blocking solution at 1:250 for 2.5 hours, extensively washed, and cover-slipped with Fluoromount-G (Southern Biotech, Birmingham, AL). Sections were photographed using NIS Elements software and a Nikon Eclipse Ti microscope. TG neurons with distinct nuclei were counted in every 5th section (16 sections/mouse) [57]. ImageJ

software (NIH, Bethesda, MD) was used to measure the size profiles at 20× magnification of 50 random neurons per animal.

2.10 Statistical Analysis

Analysis of variance (ANOVA) was employed to evaluate the difference between groups in animal studies using Prism statistical software (Graphpad Software Inc., La Jolla, CA). To adjust for multiple comparisons, the post-hoc Holm-Sidak test statistic was employed. Statistical significance was set at $p < 0.05$. Results were presented as mean ± standard error of the mean.

3. Results

3.1 Oral cancer-secreted mediators evoked functional allodynia in mice

We have previously demonstrated that oSCC is more painful than melanoma using an orthotopic xenograft mouse model [52]. Furthermore, a single injection of culture supernatant from oral cancer cell lines drives acute allodynia in mice [38], suggesting that secreted mediators within the tumor microenvironment is the primary etiology of oSCC-induced nociception. To further quantify secreted mediator-evoked nociception, we measured orofacial nociceptive behavior in response to cell line supernatant from 5 cell lines: two oSCC cell lines (i.e. HSC3, SCC9), a skin melanoma cell line (i.e. SkMel28), a dysplastic oral keratinocyte cell line (i.e. DOK), considered to be precancerous, and an immortalized non-tumorigenic keratinocyte cell line (i.e. HaCaT). As indicated by the timeline in Figure 1, mice were trained to complete an orofacial gnawing assay, dolognawmeter [16], for 4 weeks. Three baseline gnaw times were measured and then mice were injected with cell line supernatant (50 μl) into the left lateral tongue for 3 consecutive days. Three consecutive injections of supernatant were used to mimic a persistent exposure to mediators released by the cell line, without the impact of tumor infiltration. Functional allodynia, as indicated by an increase in gnaw time, was measured 1 hour after the final injection of cell line supernatant (Figure 1a). There was no difference in baseline gnaw times between groups; therefore, data was analyzed as a percent change from baseline using One-way ANOVA. Cell line supernatants from oral cancer cell lines, HSC3 and SCC9, induced a significant increase in gnaw time (87.15 ± 8.3% and 50.6 ± 6.8% respectively, $p < 0.05$; Figure 1B). In contrast, HaCaT, DOK and SkMel28 elicited no functional impairment compared to baseline gnawing (2.10 ± 5.6%, 0.19 ± 4.7%, and 12.9 ± 4.1% respectively, $p > 0.05$).

3.2 Cancer-secreted mediators recruited immune cells to the tongue microenvironment

Inflammation contributes to cancer pain [26,31,48]. Crosstalk between cancer cells and the immune system can result in an increase in pro-nociceptive cytokines and chemokines in the microenvironment [23,34]. Therefore, we quantified the magnitude of inflammatory infiltrate associated with injection of cell line supernatant into the tongue. Flow cytometry, with the gating strategy illustrated in Figure 2A, was used to characterize the immune cell types that infiltrated into the tongue tissue in response to cell line supernatant. In dissociated tongue tissue of naïve female mice, 6.6 ± 0.8% of the live cells in the tongue were CD45+ immune cells. Within the CD45+ population, six types of immune cells were detected and

quantified: 63.9 ± 1.6% CD11b+CD11c− macrophages/monocytes, 1.1 ± 0.18% CD11b +CD11c− dendritic cells, 3.5 ± 0.4% Ly6G+ neutrophils, 5.3 ± 0.6% CD3+ T cells, 2.6 ± 0.2% CD3-NK1.1+ natural killer (NK) cells, and 9.6 ± 0.4% CD3-B220+ B cells. On average, 14.7 ± 1.6% of immune cells were unidentified using our antibody panel.

Using the supernatant model of oral cancer pain, the number of infiltrating immune cells was quantified using flow cytometry twelve hours after the last of three consecutive injections of cell line supernatant into the tongue. Cell line supernatants from DOK (n = 6) and HaCaT (n = 10) cell lines did not result in any significant infiltration of CD45+ leukocytes into the tongue ($p > 0.05$) compared to naïve tongue tissue (One-way ANOVA $p > 0.05$; Figure 2B). However, HSC3 (n = 10), SCC9 (n = 10), and SkMel28 (n = 6) supernatant inoculation resulted in a significant increase in the proportion of total immune cells (CD45+) in the tongue (One-way ANOVA, $p < 0.05$; Figure 2B). Specifically, for oral cancer supernatants, there was a significant increase in the CD11b+CD11c− macrophages/ monocytes subpopulation as well as Ly6G+ neutrophils; whereas SkMel28 supernatant evoked a significant infiltration of only Ly6G+ neutrophils (One-way ANOVA, $p < 0.05$; Figure 2C). Despite a trend for an increase in T cells and B cells in response to DOK and HSC3, there was no significant difference ($p > 0.05$; Figure 2B–C).

3.3 Oral cancer-secreted mediators evoked orofacial nociceptive behavior in immune-deficient mice

Melanoma supernatant injection elicited infiltration of immune cells, despite no change in gnaw-time, suggesting that inflammation can be dissociated from nociception. Therefore, we sought to determine the contribution of inflammatory infiltrate on acute nociceptive behavior elicited by the cell line supernatant. Using the supernatant model, we compared supernatant-evoked nociception in female C57BL/6 mice to that in immune-deficient NSG™ mice. Cell line supernatants from the HSC3 induced an increase in gnaw time in both C57BL/6 and NSG™ mice (114.1 ± 41.3% and 66.4 ± 22.9% respectively, $p < 0.05$; Figure 3A), whereas, HaCaT evoked no functional impairment compared to baseline gnawing (1.17 ± 6.6% and 1.44 ± 8.2% respectively, $p > 0.05$). Two-way ANOVA analysis revealed a significant effect of treatment ($p < 0.005$) but no significant interaction between treatment and genotype ($p > 0.05$; Figure 3A).

Flow cytometry was used to measure the immune cell infiltrate in the tongue tissue from these two groups of mice. Two-way ANOVA analysis identified a significant interaction between treatment and genotype with regard to CD45+ immune cells and CD11b+ and Ly6G+ myeloid subpopulations. Consistent with previous findings, C57BL/6 mice treated with HSC3 supernatant had a significant increase in CD45+ immune cells (164.0 ± 21.1%, $p < 0.01$), CD11b+ macrophages/monocytes (91.0 ± 15.5%, $p < 0.01$), and Ly6G+ neutrophils (2345.3 ± 20.6%, $p < 0.01$) compared to HaCaT treatment. Immune-deficient NSG™ mice treated with HSC3 supernatant had no significant increase in CD45+ cells ($p > 0.05$; Figure 3B) and no significant shifts in CD45+ subpopulations (Figure 3C), which is consistent with the defective myeloid cell signaling and lack of mature lymphocytes characterizing this mouse model. These data suggest that in the absence of a functional immune system, cancer supernatant can still drive similar nociceptive behavior.

3.4 Oral cancer-secreted mediators sensitized tongue primary afferent neurons

Oral cancers are known to release mediators which interact with the microenvironment [23,53,72] and activate sensory neurons [59]. To determine if oral cancer supernatant evoked nociceptive behavior through direct activation of primary afferent neurons, we first sought to characterize the subtypes of neurons that innervate the tongue (Figure 4A). Using a retrograde tracer to identify the subpopulation of TG neurons that innervate the tongue, we determined that the majority of tongue primary afferent neurons overlap with CGRP-immunolike reactivity (IR) (64.3 ± 13.2%). Lesser subpopulations were also found to overlap with IB4-IR (13.2 ± 1.6%) and NF200-IR (31.92 ± 5.1%; Figure 4B). The size distribution of DiI+ tongue afferent neurons is shown in a histogram in Figure 4C.

Second, we performed whole cell current clamp experiments on acutely dissociated retrogradely labeled (DiI+) TG neurons to measure the effect of cell line supernatant on tongue afferent neuron excitability. Data were collected from 72 DiI+ tongue afferent neurons from 17 female C57BL/6 mice. The median cell body capacitance of these neurons was 13.15 pF (with 11.0 pF and 16.4 pF as 25^{th} and 75^{th} percentiles, respectively). There was no difference in the average capacitance of DiI+ neurons studied between groups (Table 1). Excitability was assessed before and after application of a cell line supernatant in current clamp mode using four measures: emergence of spontaneous activity, AP threshold, rheobase, and accommodation (for definitions, see *Materials and Methods*). Baseline excitability was measured followed by a 3 minute application of cell line supernatant during a ramp and hold protocol. No spontaneous activity was detected in the absence or presence of supernatant. There was no significant difference ($p > 0.05$) in baseline excitability parameters between populations of neurons prior to supernatant application; therefore data were analyzed as a percent change from baseline using a One-way ANOVA with Holm Sidak post hoc comparisons. Application of HSC3 supernatant resulted in a significantly more negative AP threshold (−15.38 ± 7.0%, $p < 0.05$; Figure 5A), a significant decrease in rheobase (−29.60 ± 5.5%, $p < 0.05$; Figure 5B), and a significant increase in accommodation (308.7 ± 70.6%, $p < 0.01$; Figure 5C,D). There were also changes in passive and active electrophysiological properties associated with the HSC3-induced increase in excitability (Table 1). A significant HSC3-induced depolarization of the membrane potential (V_m, $p < 0.05$) was detected. This was associated with a significant decrease in input resistance (R_{in}, $p < 0.05$). In contrast, tongue afferent neurons showed no change in excitability parameters following a 3-minute application of supernatants from DOK, SkMel28, or HaCaT cell lines and thus were considered unresponsive (Figure 5). Consistent with the supernatant-evoked nociceptive behavior, these data demonstrate that only mediators secreted from oral cancer, compared to the other cell lines tested, directly sensitized tongue primary afferent neurons.

3.5 Analysis of cancer cell line supernatant protein contents revealed multiple pro-inflammatory and pro-nociceptive mediators

The orofacial behavior and flow cytometry analyses allowed us to classify the cancer-associated cell lines into 3 phenotypes: nociceptive/inflammatory (HSC3, SCC9), non-nociceptive/inflammatory (SkMel28), and non-nociceptive/non-inflammatory (DOK). We used a cytokine magnetic bead panel to quantify 38 protein mediators released from these cell lines to disambiguate mediators driving nociception versus inflammation in the setting

of cancer. Thirty-five of the mediators measured were present in the cell line supernatants from HaCaT, DOK, HSC3, SCC9, and SkMel28, while 3 cytokines were below the range of detection based on the internal standards provided by the manufacturer. We calculated the fold change for each cytokine in DOK, HSC3, SCC9, and SkMel28 compared to that detected in the supernatant from HaCaT. Of the 35 mediators evaluated, 9 mediators showed a ≥ 10 fold increase compared to HaCaT (Figure 6). To select mediators associated with nociception, we identified those proteins increased in oral cancer cell lines, HSC3 and SCC9, but not SkMel28 or DOK. Two-way ANOVA repeated measure found a significant interaction between cell line supernatant and the 9 elevated proteins. Dunnett's post hoc analysis revealed that only granulocyte macrophage-colony stimulating factor (GM-CSF) and tumor necrosis factor alpha (TNFα) were significantly elevated ($p < 0.05$) in both oral cancer cell line supernatants compared to HaCaT supernatant (Figure 6). These data suggest that GM-CSF and TNFα may be responsible for the nociceptive component of oral cancer supernatant. TNFα is a pro-inflammatory chemokine involved in lymphocyte recruitment [74], can alter neuronal excitability and has been implicated in the mechanical allodynia associated with neuropathic pain [20,63,70]. GM-CSF is a hematopoietic stimulating factor that acts on myeloid and tumor cells [27]. GM-CSF has shown to be increased in T lymphocytes after nerve injury [17] and when injected directly into the skin results in nociceptive behavior [61]. However, because TNFα was identified as a primary mediator upregulated with anti-PD-1/PD-L1 therapy [13,41], we will focus on TNFα for subsequent experiments.

3.6 Oral functional allodynia developed during 4NQO-induced carcinogenesis

The objective of the *in vitro* experiments using cell line supernatants was to measure the nociceptive and inflammatory components of oral cancer in the absence of carcinogenesis and tumor burden. The data from the supernatant model suggests that inflammation and nociception are dissociable. However, mediators from oral cancer result in both nociception and immune cell infiltration. Next, we sought to quantify cancer-induced inflammation and nociception during oral cancer development and progression using a mouse model for tongue squamous cell carcinoma. Water-soluble quinoline derivative, 4-nitroquinoline-1-oxide (4NQO), was initially developed as a chemotherapeutic agent but has been shown to produce both dysplasia and oSCC in mice [29,60]. The molecular events in the 4NQO-induced oSCC closely resemble those observed in human head and neck carcinoma [77,78]. For this study, mice were trained in the dolognawmeter and given 4NQO treatment (100μg/mL, n = 35) or the equivalent dilution of the vehicle, propylene glycol (n = 10), in the drinking water for 16 weeks. The mice were then monitored weekly under light anesthesia for tumor size, incidence and location for an additional 12 weeks. Nociceptive behavior was also measured weekly (Figure 7A). By 28 weeks, all mice treated with 4NQO showed pathologic changes in the tongue. Moderate dysplastic changes were detected in 20.8% of mice. Severe dysplasia and carcinoma *in situ* were detected in 45.9% and squamous cell carcinoma was detected in 33.3% of the mice (Figure 7B). Control mice treated with propylene glycol showed no pathologic changes compared to naïve mice. Mice that developed oSCC experienced functional allodynia beginning at 4–6 weeks post-4NQO carcinogenesis treatment and continued to worsen for the remaining 6 weeks (Two-way ANOVA, $p < 0.05$; Figure 8). Mice with severe dysplasia showed significant increases in

gnaw time by 11 weeks post-4NQO carcinogenesis treatment compared to gnaw times in control treated mice ($p < 0.05$; Figure 8).

3.7 Increased immune cell infiltrate is associated with 4NQO-induced oSCC

Next, we quantified and characterized the immune cell infiltrate associated with 4NQO-induced carcinogenesis. Using the antibody panel and flow cytometry gating strategy illustrated in Figure 4, we measured the percent of CD45+ cells in the tongue tissue from mice with 4NQO-induced moderate dysplasia (n = 6 mice), severe dysplasia (n = 10 mice), and oSCC (n = 10 mice). Changes in CD45+ cell infiltration with treatment were compared to those values from tongue tissue in vehicle-treated mice (n = 10 mice). A significant increase in CD45+ cells was detected only in mice with 4NQO-induced oSCC (89.9 ± 2.5%, One-way ANOVA $p < 0.05$; Figure 9A). Further characterization of the subpopulations of CD45+ cells revealed a significant increase in the percent of Ly6G+ neutrophils (338.5 ± 53.6%, $p < 0.05$) and CD3+ T cells (425.9 ± 45.2%, $p < 0.05$) present in the tongue tissue from mice with 4NQO-induced oSCC (Figure 9B). The increase in CD3+ T cells was reflective of a significant increase in CD3+CD4+ T helper cells (425.9 ± 45.3%, $p < 0.05$; Figure 9B inset). These data are consistent with previous immunohistological studies that quantified changes in leukocyte populations in 4NQO-treated mice during carcinogenesis [10].

3.8 Neuronal sensitization in trigeminal tongue afferent neurons during 4NQO-induced carcinogenesis

The cell line supernatant model results suggested that oral cancer cells release mediators that can sensitize the tongue afferent neurons directly as well as drive an inflammatory response in the tongue microenvironment. Based on the nociceptive behavior and immune cell infiltrate associated with 4NQO-induced oSCC, we sought to determine the impact of carcinogenesis on the baseline excitability of primary afferent neurons innervating the cancer microenvironment. Using whole cell current clamp electrophysiology, we measured baseline excitability in 99 retrogradely labeled (DiI+) tongue afferent neurons from vehicle-treated mice (n = 4 mice) and mice with 4NQO-induced moderate dysplasia (n = 4 mice), severe dysplasia (n = 4 mice), and oSCC (n = 6 mice). Mouse tongues were back-labeled with the retrograde tracer 10 days prior to 4NQO treatment. There was no difference in the size distribution of acutely dissociated, retrogradely labeled neurons from vehicle or 4NQO-treated mice (Table 2). DiI+ neurons from mice with moderate dysplasia (n = 36 neurons) showed no change in membrane potential (Figure 10A) or baseline excitability, as measured by rheobase (Figure 10B) and AP threshold (Figure 10C), compared to neurons from vehicle-treated mice (n = 21 neurons). However, DiI+ neurons from mice with 4NQO-induced severe dysplasia (n = 24 neurons) and oSCC (n = 18 neurons) had more depolarized resting membrane potential (−11.2 ± 3.9% and −15.5 ± 3.9%, respectively, $p < 0.05$) and significantly decreased rheobase (−24.4 ± 5.0% and −38.9 ± 4.9%, respectively, $p < 0.05$; Figure 10B) and a more hyperpolarized AP threshold (−30.0 ± 3.7% and −42.1 ± 3.4%, respectively, $p < 0.05$; Figure 10C). Additionally, spontaneous activity was detected in 6 neurons from 4NQO-induced oSCC mice only and no additional data were collected from these neurons. Using a 4 millisecond square pulse to evoke an AP, the active electrophysiological parameters, as defined in Figure 10D, were compared between neurons

from vehicle and 4NQO-treated mice (Table 2). Given the more depolarized resting membrane potential, the peak amplitude of the AP (overshoot) was significantly smaller (Two-way ANOVA, $p < 0.05$) in neurons from mice with 4NQO-induced oSCC (42.6 ± 3.6 mV) compared to neurons from vehicle-treated mice (61.4 ± 1.8 mV). While there was no change in the afterhyperpolarization (AHP) magnitude between groups ($p > 0.05$), the AHP time constant (τ) of decay was significantly increased (One-way ANOVA, $p < 0.05$) in neurons from mice with 4NQO-induced oSCC (127.6 ± 16.8 ms) compared to neurons from vehicle-treated mice (61.7 ± 17.7 ms) suggesting increased AP firing potential [47]. Furthermore, input resistance was lower in neurons from mice with 4NQO-induced oSCC (1389.3 ± 361.0 mω) compared to neurons from vehicle-treated mice (1704.6 ± 212.8 mω); however the groups were not statistically different (One-way ANOVA, $p > 0.05$).

3.9 TNFα protein increased in 4NQO-induced oSCC microenvironment

Our data indicates that human oral cancer cell lines produced high concentration of the nociceptive and chemotactic cell signaling protein, TNFα, compared to non-nociceptive dysplasia and melanoma cell lines. Furthermore, high levels of TNFα have been documented in human oSCC [51]. We hypothesized that this mediator was important for the nociceptive behavior associated with oral cancer. We used an enzyme immunoassay to quantify the concentration of TNFα in homogenized tongue tissue from vehicle-treated mice as well as mice with 4NQO-induced dysplasia and oSCC. Consistent with previous studies [24,54] and our data in the human cancer cells lines, there was a significant increase in TNFα (3644.3 ± 22.1%, Student's *t* test, $p < 0.01$) in 4NQO-induced oSCC tongue tissue compared to dysplastic tongue tissue (Figure 11A). We then examined the expression of TNFα receptors in trigeminal tongue afferent neurons. TNFα can bind two receptors, TNF receptor type 1 (TNFR1) and TNF receptor type 2 (TNFR2). We used TG sections from retrogradely labeled mice to locate TNFR1 and TNFR2 in tongue primary afferent neurons. Cytoplasmic TNFR1-IR and TNFR-IR were present in almost all (> 90%) DiI+ neurons (Figure 11B). Increased levels of TNFα in the microenvironment suggest increased binding to receptors on primary afferent neurons innervating the tongue.

3.10 Anti-TNFα co-injection with oral cancer cell line supernatant abolished functional allodynia in mice

The source of TNFα measured in the 4NQO-treated tongue tissue could originate from tumor cells [51], stromal cells [4,71], or infiltrating immune cells [8,21]. Furthermore, TNFα inhibition in oral cancer cell lines has been previously demonstrated to reduce cell viability, activate apoptosis, and inhibit migration [33]. To understand the direct impact of TNFα signaling on cancer-induced nociception, we utilized the supernatant model with a TNF-TNFR signaling inhibitor, C87, which directly binds to TNFα to block TNFα-stimulated activity [45]. Mice were co-injected with oral cancer cell line supernatant and C87 (5 mg/kg; HSC3+C87, SCC9+C87) into the anterior portion of the tongue for 3 consecutive days. Injections of HSC3 or SCC9 with the vehicle (0.02% DMSO, HSC3+vehicle, SCC9+vehicle) and C87 with normal culture media (DMEM+C87) were also performed for comparison. Functional allodynia was measured 1 hour after the final injection (Figure 12A). Consistent with previous experiments, One-way ANOVA analysis indicated that HSC3+vehicle and SCC9+vehicle induced significant increases in gnaw time

(104.1 ± 23.5% and 70.6 ± 10.6% respectively, $p < 0.05$). In contrast, co-injection of HSC3+C87 and SCC9+C87 elicited no significant functional impairment compared to baseline gnawing (23.8 ± 8.7% and 5.8 ± 17.22% respectively, $p > 0.05$) (Figure 12A). Similarly, injection of DMEM+C87 also did not affect gnaw time (−3.28 ± 10.5%, $p > 0.05$).

To quantify the magnitude of TNFα-induced inflammatory infiltrate evoked by the cancer supernatant, immune cells were quantified in tongue tissue from mice. There was a significant increase in CD45+ immune cells in mice treated with HSC3+vehicle (13.6 ± 3.3%) and HSC3+C87 (24.1 ± 0.3%) compared to DMEM+C87 (11.1 ± 0.53%, One-way ANOVA, $p < 0.05$; Figure 12B). Analysis of the subpopulations of CD45+ leukocytes revealed a significant increase in Ly6G+ neutrophils in response to HSC3+C87 (One-way ANOVA, $p < 0.05$; Figure 12C). However, C87+DMEM also resulted in a significant increase in Ly6G+ neutrophils compared to DMEM alone (6.4 ± 1.4% and 0.53 ± 0.1%, $p < 0.05$; data not shown) suggesting C87 disrupted TNFα signaling in response to injection or the compound itself elicited an innate inflammatory reaction [64]. There was also a significant decrease in CD3+ T cells in both HSC3+C87 (−33.9 ± 11.2 %) and SCC9+C87 (−42.3 ± 7.7%) groups compared to HSC3+vehicle and SCC9+vehicle respectively ($p < 0.05$; Figure 12C).

4. Discussion

In the present study, we demonstrated that TNFα from oral cancer induces nociception. Correlations between tissue levels of TNFα and pain and hyperalgesia have been noted in a number of painful diseases [2,62,65]. TNFα was previously identified in oSCC from patients [51] and as a primary cytokine in transformed epithelium of 4NQO-treated mice at both the mRNA and protein level [24]; however, the role of TNFα in oral cancer-induced nociception has not been studied. In a bone cancer pain model, systemic injection of a TNFα antagonist partially blocked mechanical hyperalgesia, indicating that local production of TNFα may contribute to tumor-induced nociception [12,69]. Additionally, Constantin et al demonstrated a significant contribution of TNFα to the development of cancer-induced thermal hyperalgesia in a soft tissue tumor model [12]. None of these studies, however, addressed the contribution of TNFα in regard to the occurrence and mechanisms of inflammation associated with cancer-induced nociception.

Inflammation is a hallmark of cancer [11]. While the role of inflammation in cancer pain has been unclear and our study does not conclusively answer the question, our results suggest that cancer pain can develop without an inflammatory response. To begin, oral cancer supernatant induced similar levels of nociception in immune-competent and immune-deficient mice. The melanoma supernatant mouse model exhibited inflammation but no nociception. Mice with 4NQO-induced severe dysplasia, the final precancerous step before cancer, demonstrated significant nociceptive behavior in the absence of a significant inflammatory response. Oral cancers typically induce an inflammatory response through the production and secretion of mediators, including TNFα [3,21,22,43]. Inhibition of TNFα signaling with C87 abolished nociception and decreased the number of CD3+ T cells infiltrating into the tongue. This loss of TNFα-induced T cell infiltration is consistent with clinical trials showing that a single intravenous infusion of monoclonal antibody against

TNFα dramatically decreased the number of epidermal CD3+ T cells [25]. The number of neutrophils, which increases significantly in response to cancer supernatant, was not affected by the inhibition of TNFα signaling. The lack of change in neutrophil number in response to C87 was unexpected given that generation, accumulation, and function of neutrophils is thought to depend on TNF-TNFR2 signaling [80]. Furthermore, Nadeau and colleagues demonstrated that neutrophils are recruited in a TNFα-dependent fashion after peripheral nerve injury [49]. However, additional mediators released from oral cancer are capable of maintaining the neutrophil number in the cancer microenvironment in response to oral cancer supernatant, including GM-CSF and IL-8, which were shown to be released in high concentration by the oral cancer cell lines and are known to attract neutrophils [5,18]. A lack of nociceptive behavior in the presence of a significant increase in neutrophils suggests that neutrophils do not play a significant role in oral cancer supernatant-induced nociceptive behavior or possibly that neutrophils mediate analgesia.

The impact of inflammation on cancer pain has eluded the field due to the challenges of generating a physiologically relevant animal cancer model. The xenograft rodent models simulate the rapid growth, tissue destruction and pain of cancers in humans; however, they do not recapitulate the response of the immune system to the progressive stages of carcinogenesis. Despite this limitation, the xenograft model suggests that cancer pain is a form of nociceptive pain, which is distinguishable from inflammatory pain [28,32]. The location of cancer inoculation also introduces a variable that deviates from the natural condition. Given that paw withdrawal is a well-established nociceptive assay and accepted as reproducible by other investigators, the hindpaw is a standard site for the study of cancer pain [1,6,7,52,68]. However, the glabrous skin is a rare site for squamous cell carcinoma and the oral cavity differs greatly in gross and microscopic anatomy. The interplay between oSCC, the surrounding stroma and infiltrating immune system is thought to be critical for physiologically relevant tumor biology [19]. Therefore, our group has utilized two mouse models to address these inconsistencies. We have demonstrated here and previously [52,75,76] that oral cancer cells release protein mediators that directly impact the cancer microenvironment. The orthotopic injection of cancer supernatant allows for the analysis of the nociceptive effect of secreted mediators without the impact of tumor burden and systemic illness that accompany carcinogenesis. The 4NQO-induced carcinogenesis model best mimics the natural disease progression of oral cancer in humans; 4NQO causes DNA adduct formation similar to carcinogens found in tobacco [66]. Ten to 20 weeks of treatment with 4NQO produces pre-neoplastic (*i.e.,* dysplasia) and neoplastic (*i.e.*, SCC) lesions in mice that exhibit similar histological, molecular, and chromosomal alterations observed in human carcinogenesis [60,66]. We have demonstrated previously [38] and in this study that it is a suitable model to study the development of cancer pain that persists for months. In tandem with our validated anatomically relevant operant assay [16] measuring pain-induced functional impairment, these two models better reflect clinical oral cancer-induced nociception and inflammation than previous animal models.

We also leveraged these two cancer models to study the impact of cancer on excitability of neurons that innervate the tongue. The 4NQO model provided the most clinically meaningful information because afferent neuronal plasticity would occur in parallel with carcinogenesis. Afferent neurons innervating the tongues of 4NQO-treated mice with severe

dysplasia and oSCC had depolarized resting membrane potential, a decrease in rheobase, and a more hyperpolarized AP threshold. One possible mechanism to explain neuronal hyperexcitability in this model is the introduction of an active depolarizing current such as an increase in persistent Na^+ current or a depolarizing shift in activation of a hyperpolarization-activated cyclic nucleotide–gated (HCN) channel [73]. TNFα can sensitize primary afferents in naïve or tumor-bearing mice [69]. We demonstrated that tongue primary afferent neurons express both TNFR1 and TNFR2. The underlying mechanism of TNFα-induced neuronal excitability is thought to be due to a shift in voltage gated Na^+ channel activation and sensitization of transient receptor potential (TRP) channels [15,30]. Future studies will assess changes in these receptors at the protein level and functionally to understand the ionic mechanism(s) underlying neuronal excitability and the role for TNFα signaling on the primary afferent neuron during oral carcinogenesis. These results also provide further evidence that secreted nociceptive mediators within the tumor microenvironment is most likely the primary etiology of oral cancer pain [37,39,52,75,76].

In summary, we have characterized nociception and inflammation in supernatant and chemical carcinogenesis models of oral cancer pain. We demonstrate that inflammation is a prominent component of oral cancer, but oral cancer-induced nociception is not dependent on the inflammatory infiltrate. However, the inflammatory cytokine, TNFα, was discovered to be a key mediator in oral cancer-induced nociception. With new immunotherapy treatments designed to enhance the immune response in the cancer microenvironment, these data highlight the need for further investigation in neural-immune communication in cancer pain.

Acknowledgments

We thank Mr. Yogin Patel as well as Dr. David Levy and the New York University College of Dentistry Flow Cytometry Facility for their technical contributions. We thank Dr. Brad Aouizerat for his invaluable feedback during the preparation of this manuscript. The IASP 2014 John J. Bonica Training Fellowship (N.N.S.) and the NIH/NIDCR R01DE019796 and R01DE025393 (B.L.S.) supported this work. There are no conflicts of interest.

References

1. Asai H, Ozaki N, Shinoda M, Nagamine K, Tohnai I, Ueda M, Sugiura Y. Heat and mechanical hyperalgesia in mice model of cancer pain. Pain. 2005; 117(1–2):19–29. [PubMed: 16043290]
2. Barnes PF, Chatterjee D, Brennan PJ, Rea TH, Modlin RL. Tumor necrosis factor production in patients with leprosy. Infect Immun. 1992; 60(4):1441–1446. [PubMed: 1548069]
3. Benoliel R, Epstein J, Eliav E, Jurevic R, Elad S. Orofacial pain in cancer: part I--mechanisms. Journal of dental research. 2007; 86(6):491–505. [PubMed: 17525348]
4. Botero JE, Contreras A, Parra B. Profiling of inflammatory cytokines produced by gingival fibroblasts after human cytomegalovirus infection. Oral Microbiol Immunol. 2008; 23(4):291–298. [PubMed: 18582328]
5. Brandau S, Dumitru CA, Lang S. Protumor and antitumor functions of neutrophil granulocytes. Semin Immunopathol. 2013; 35(2):163–176. [PubMed: 23007469]
6. Brigatte P, Sampaio SC, Gutierrez VP, Guerra JL, Sinhorini IL, Curi R, Cury Y. Walker 256 tumor-bearing rats as a model to study cancer pain. J Pain. 2007; 8(5):412–421. [PubMed: 17287145]
7. Cain DM, Wacnik PW, Eikmeier L, Beitz A, Wilcox GL, Simone DA. Functional interactions between tumor and peripheral nerve in a model of cancer pain in the mouse. Pain Med. 2001; 2(1): 15–23. [PubMed: 15102313]

8. Chatzidakis I, Mamalaki C. T cells as sources and targets of TNF: implications for immunity and autoimmunity. Curr Dir Autoimmun. 2010; 11:105–118. [PubMed: 20173390]
9. Chen X, Fosco D, Kline DE, Meng L, Nishi S, Savage PA, Kline J. PD-1 regulates extrathymic regulatory T-cell differentiation. Eur J Immunol. 2014; 44(9):2603–2616. [PubMed: 24975127]
10. Chu M, Su YX, Wang L, Zhang TH, Liang YJ, Liang LZ, Liao GQ. Myeloid-derived suppressor cells contribute to oral cancer progression in 4NQO-treated mice. Oral diseases. 2012; 18(1):67–73. [PubMed: 21883708]
11. Colotta F, Allavena P, Sica A, Garlanda C, Mantovani A. Cancer-related inflammation, the seventh hallmark of cancer: links to genetic instability. Carcinogenesis. 2009; 30(7):1073–1081. [PubMed: 19468060]
12. Constantin CE, Mair N, Sailer CA, Andratsch M, Xu ZZ, Blumer MJ, Scherbakov N, Davis JB, Bluethmann H, Ji RR, Kress M. Endogenous tumor necrosis factor alpha (TNFalpha) requires TNF receptor type 2 to generate heat hyperalgesia in a mouse cancer model. The Journal of neuroscience : the official journal of the Society for Neuroscience. 2008; 28(19):5072–5081. [PubMed: 18463260]
13. Curran MA, Montalvo W, Yagita H, Allison JP. PD-1 and CTLA-4 combination blockade expands infiltrating T cells and reduces regulatory T and myeloid cells within B16 melanoma tumors. Proc Natl Acad Sci U S A. 2010; 107(9):4275–4280. [PubMed: 20160101]
14. Currie GL, Sena ES, Fallon MT, Macleod MR, Colvin LA. Using animal models to understand cancer pain in humans. Curr Pain Headache Rep. 2014; 18(6):423. [PubMed: 24760492]
15. Czeschik JC, Hagenacker T, Schafers M, Busselberg D. TNF-alpha differentially modulates ion channels of nociceptive neurons. Neurosci Lett. 2008; 434(3):293–298. [PubMed: 18314270]
16. Dolan JC, Lam DK, Achdjian SH, Schmidt BL. The dolognawmeter: a novel instrument and assay to quantify nociception in rodent models of orofacial pain. Journal of neuroscience methods. 2010; 187(2):207–215. [PubMed: 20096303]
17. Draleau K, Maddula S, Slaiby A, Nutile-McMenemy N, De Leo J, Cao L. Phenotypic Identification of Spinal Cord-Infiltrating CD4+ T Lymphocytes in a Murine Model of Neuropathic Pain. J Pain Relief. 2014; (Suppl 3):003. [PubMed: 25143871]
18. Dumitru CA, Lang S, Brandau S. Modulation of neutrophil granulocytes in the tumor microenvironment: mechanisms and consequences for tumor progression. Semin Cancer Biol. 2013; 23(3):141–148. [PubMed: 23485549]
19. Dvorak HF, Nagy JA, Feng D, Brown LF, Dvorak AM. Vascular permeability factor/vascular endothelial growth factor and the significance of microvascular hyperpermeability in angiogenesis. Curr Top Microbiol Immunol. 1999; 237:97–132. [PubMed: 9893348]
20. Empl M, Renaud S, Erne B, Fuhr P, Straube A, Schaeren-Wiemers N, Steck AJ. TNF-alpha expression in painful and nonpainful neuropathies. Neurology. 2001; 56(10):1371–1377. [PubMed: 11376190]
21. Fridlender ZG, Albelda SM. Tumor-associated neutrophils: friend or foe? Carcinogenesis. 2012; 33(5):949–955. [PubMed: 22425643]
22. Friedman R. Pain at the cellular level: the role of the cytokine tumor necrosis factor-alpha. Reg Anesth Pain Med. 2000; 25(2):110–112. [PubMed: 10746525]
23. Fukuyama T, Ichiki Y, Yamada S, Shigematsu Y, Baba T, Nagata Y, Mizukami M, Sugaya M, Takenoyama M, Hanagiri T, Sugio K, Yasumoto K. Cytokine production of lung cancer cell lines: Correlation between their production and the inflammatory/immunological responses both in vivo and in vitro. Cancer Sci. 2007; 98(7):1048–1054. [PubMed: 17511773]
24. Gannot G, Buchner A, Keisari Y. Interaction between the immune system and tongue squamous cell carcinoma induced by 4-nitroquinoline N-oxide in mice. Oral Oncol. 2004; 40(3):287–297. [PubMed: 14747060]
25. Gottlieb AB, Masud S, Ramamurthi R, Abdulghani A, Romano P, Chaudhari U, Dooley LT, Fasanmade AA, Wagner CL. Pharmacodynamic and pharmacokinetic response to anti-tumor necrosis factor-alpha monoclonal antibody (infliximab) treatment of moderate to severe psoriasis vulgaris. J Am Acad Dermatol. 2003; 48(1):68–75. [PubMed: 12522373]

26. Hald A, Nedergaard S, Hansen RR, Ding M, Heegaard AM. Differential activation of spinal cord glial cells in murine models of neuropathic and cancer pain. European journal of pain. 2009; 13(2): 138–145. [PubMed: 18499488]
27. Hamilton JA. Colony-stimulating factors in inflammation and autoimmunity. Nat Rev Immunol. 2008; 8(7):533–544. [PubMed: 18551128]
28. Harano N, Ono K, Hidaka K, Kai A, Nakanishi O, Inenaga K. Differences between orofacial inflammation and cancer pain. Journal of dental research. 2010; 89(6):615–620. [PubMed: 20332329]
29. Hawkins BL, Heniford BW, Ackermann DM, Leonberger M, Martinez SA, Hendler FJ. 4NQO carcinogenesis: a mouse model of oral cavity squamous cell carcinoma. Head Neck. 1994; 16(5): 424–432. [PubMed: 7960739]
30. Hensellek S, Brell P, Schaible HG, Brauer R, Segond von Banchet G. The cytokine TNFalpha increases the proportion of DRG neurones expressing the TRPV1 receptor via the TNFR1 receptor and ERK activation. Mol Cell Neurosci. 2007; 36(3):381–391. [PubMed: 17851089]
31. Honore P, Luger NM, Sabino MA, Schwei MJ, Rogers SD, Mach DB, O'Keefe PF, Ramnaraine ML, Clohisy DR, Mantyh PW. Osteoprotegerin blocks bone cancer-induced skeletal destruction, skeletal pain and pain-related neurochemical reorganization of the spinal cord. Nat Med. 2000; 6(5):521–528. [PubMed: 10802707]
32. Honore P, Rogers SD, Schwei MJ, Salak-Johnson JL, Luger NM, Sabino MC, Clohisy DR, Mantyh PW. Murine models of inflammatory, neuropathic and cancer pain each generates a unique set of neurochemical changes in the spinal cord and sensory neurons. Neuroscience. 2000; 98(3):585–598. [PubMed: 10869852]
33. Iulia Irimie A, Braicu C, Zanoaga O, Pileczki V, Soritau O, Berindan-Neagoe I, Septimiu Campian R. Inhibition of tumor necrosis factor alpha using RNA interference in oral squamous cell carcinoma. J BUON. 2015; 20(4):1107–1114. [PubMed: 26416064]
34. Jimenez Andrade, JM., Mantyh, P. Cancer Pain: From the Development of Mouse Models to Human Clinical Trials. In: Kruger, L., Light, AR., editors. Translational Pain Research: From Mouse to Man. Boca Raton, FL: 2010.
35. Junger H, Sorkin LS. Nociceptive and inflammatory effects of subcutaneous TNFalpha. Pain. 2000; 85(1–2):145–151. [PubMed: 10692613]
36. Kanojia D, Vaidya MM. 4-nitroquinoline-1-oxide induced experimental oral carcinogenesis. Oral Oncol. 2006; 42(7):655–667. [PubMed: 16448841]
37. Kolokythas A, Cox DP, Dekker N, Schmidt BL. Nerve growth factor and tyrosine kinase A receptor in oral squamous cell carcinoma: is there an association with perineural invasion? J Oral Maxillofac Surg. 2010; 68(6):1290–1295. [PubMed: 20363547]
38. Lam DK, Dang D, Zhang J, Dolan JC, Schmidt BL. Novel animal models of acute and chronic cancer pain: a pivotal role for PAR2. The Journal of neuroscience : the official journal of the Society for Neuroscience. 2012; 32(41):14178–14183. [PubMed: 23055487]
39. Lam DK, Schmidt BL. Serine proteases and protease-activated receptor 2-dependent allodynia: a novel cancer pain pathway. Pain. 2010; 149(2):263–272. [PubMed: 20189717]
40. Lei ZG, Ren XH, Wang SS, Liang XH, Tang YL. Immunocompromised and immunocompetent mouse models for head and neck squamous cell carcinoma. Onco Targets Ther. 2016; 9:545–555. [PubMed: 26869799]
41. Levingston CA, Young MR. Transient immunological and clinical effectiveness of treating mice bearing premalignant oral lesions with PD-1 antibodies. Int J Cancer. 2017; 140(7):1609–1619. [PubMed: 27914100]
42. Li Y, Li F, Jiang F, Lv X, Zhang R, Lu A, Zhang G. A Mini-Review for Cancer Immunotherapy: Molecular Understanding of PD-1/PD-L1 Pathway & Translational Blockade of Immune Checkpoints. Int J Mol Sci. 2016; 17(7)
43. Lu H, Ouyang W, Huang C. Inflammation, a key event in cancer development. Mol Cancer Res. 2006; 4(4):221–233. [PubMed: 16603636]
44. Ma F, Zhang L, Oz HS, Mashni M, Westlund KN. Dysregulated TNFalpha promotes cytokine proteome profile increases and bilateral orofacial hypersensitivity. Neuroscience. 2015; 300:493–507. [PubMed: 26033565]

45. Ma L, Gong H, Zhu H, Ji Q, Su P, Liu P, Cao S, Yao J, Jiang L, Han M, Ma X, Xiong D, Luo HR, Wang F, Zhou J, Xu Y. A novel small-molecule tumor necrosis factor alpha inhibitor attenuates inflammation in a hepatitis mouse model. J Biol Chem. 2014; 289(18):12457–12466. [PubMed: 24634219]
46. Malin SA, Davis BM, Molliver DC. Production of dissociated sensory neuron cultures and considerations for their use in studying neuronal function and plasticity. Nat Protoc. 2007; 2(1): 152–160. [PubMed: 17401349]
47. Manuel M, Meunier C, Donnet M, Zytnicki D. The afterhyperpolarization conductance exerts the same control over the gain and variability of motoneurone firing in anaesthetized cats. J Physiol. 2006; 576(Pt 3):873–886. [PubMed: 16931549]
48. Mercadante S, Fulfaro F, Casuccio A. A randomised controlled study on the use of anti-inflammatory drugs in patients with cancer pain on morphine therapy: effects on dose-escalation and a pharmacoeconomic analysis. Eur J Cancer. 2002; 38(10):1358–1363. [PubMed: 12091067]
49. Nadeau S, Filali M, Zhang J, Kerr BJ, Rivest S, Soulet D, Iwakura Y, de Rivero Vaccari JP, Keane RW, Lacroix S. Functional recovery after peripheral nerve injury is dependent on the pro-inflammatory cytokines IL-1beta and TNF: implications for neuropathic pain. The Journal of neuroscience : the official journal of the Society for Neuroscience. 2011; 31(35):12533–12542. [PubMed: 21880915]
50. Pandiyan P, Bhaskaran N, Zhang Y, Weinberg A. Isolation of T cells from mouse oral tissues. Biol Proced Online. 2014; 16(1):4. [PubMed: 24612879]
51. Parks RR, Yan SD, Huang CC. Tumor necrosis factor-alpha production in human head and neck squamous cell carcinoma. Laryngoscope. 1994; 104(7):860–864. [PubMed: 7517483]
52. Pickering V, Jay Gupta R, Quang P, Jordan RC, Schmidt BL. Effect of peripheral endothelin-1 concentration on carcinoma-induced pain in mice. European journal of pain. 2008; 12(3):293–300. [PubMed: 17664075]
53. Quan J, Morrison NA, Johnson NW, Gao J. MCP-1 as a potential target to inhibit the bone invasion by oral squamous cell carcinoma. J Cell Biochem. 2014; 115(10):1787–1798. [PubMed: 24905457]
54. Rakowicz-Szulczynska EM, McIntosh DG, Smith M. Growth factor-mediated mechanisms of nicotine-dependent carcinogenesis. Carcinogenesis. 1994; 15(9):1839–1846. [PubMed: 7923576]
55. Reyes-Gibby CC, Anderson KO, Merriman KW, Todd KH, Shete SS, Hanna EY. Survival patterns in squamous cell carcinoma of the head and neck: pain as an independent prognostic factor for survival. J Pain. 2014; 15(10):1015–1022. [PubMed: 25043982]
56. Schafers M, Sorkin L. Effect of cytokines on neuronal excitability. Neurosci Lett. 2008; 437(3): 188–193. [PubMed: 18420346]
57. Schmalbruch H. The number of neurons in dorsal root ganglia L4–L6 of the rat. Anat Rec. 1987; 219(3):315–322. [PubMed: 3322108]
58. Schmidt BL. The neurobiology of cancer pain. The Neuroscientist : a review journal bringing neurobiology, neurology and psychiatry. 2014; 20(5):546–562.
59. Schmidt BL, Hamamoto DT, Simone DA, Wilcox GL. Mechanism of cancer pain. Molecular interventions. 2010; 10(3):164–178. [PubMed: 20539035]
60. Schoop RA, Noteborn MH, Baatenburg de Jong RJ. A mouse model for oral squamous cell carcinoma. J Mol Histol. 2009; 40(3):177–181. [PubMed: 19685146]
61. Schweizerhof M, Stosser S, Kurejova M, Njoo C, Gangadharan V, Agarwal N, Schmelz M, Bali KK, Michalski CW, Brugger S, Dickenson A, Simone DA, Kuner R. Hematopoietic colony-stimulating factors mediate tumor-nerve interactions and bone cancer pain. Nat Med. 2009; 15(7): 802–807. [PubMed: 19525966]
62. Shafer DM, Assael L, White LB, Rossomando EF. Tumor necrosis factor-alpha as a biochemical marker of pain and outcome in temporomandibular joints with internal derangements. J Oral Maxillofac Surg. 1994; 52(8):786–791. discussion 791–782. [PubMed: 8040729]
63. Sorkin LS, Doom CM. Epineurial application of TNF elicits an acute mechanical hyperalgesia in the awake rat. J Peripher Nerv Syst. 2000; 5(2):96–100. [PubMed: 10905468]
64. Sugawara S, Uehara A, Tamai R, Takada H. Innate immune responses in oral mucosa. Journal of endotoxin research. 2002; 8(6):465–468. [PubMed: 12697091]

65. Tak PP, Smeets TJ, Daha MR, Kluin PM, Meijers KA, Brand R, Meinders AE, Breedveld FC. Analysis of the synovial cell infiltrate in early rheumatoid synovial tissue in relation to local disease activity. Arthritis Rheum. 1997; 40(2):217–225. [PubMed: 9041933]
66. Tang XH, Knudsen B, Bemis D, Tickoo S, Gudas LJ. Oral cavity and esophageal carcinogenesis modeled in carcinogen-treated mice. Clinical cancer research : an official journal of the American Association for Cancer Research. 2004; 10(1 Pt 1):301–313. [PubMed: 14734483]
67. van den Beuken-van Everdingen MH, de Rijke JM, Kessels AG, Schouten HC, van Kleef M, Patijn J. Prevalence of pain in patients with cancer: a systematic review of the past 40 years. Ann Oncol. 2007; 18(9):1437–1449. [PubMed: 17355955]
68. Wacnik PW, Eikmeier LJ, Ruggles TR, Ramnaraine ML, Walcheck BK, Beitz AJ, Wilcox GL. Functional interactions between tumor and peripheral nerve: morphology, algogen identification, and behavioral characterization of a new murine model of cancer pain. The Journal of neuroscience : the official journal of the Society for Neuroscience. 2001; 21(23):9355–9366. [PubMed: 11717369]
69. Wacnik PW, Eikmeier LJ, Simone DA, Wilcox GL, Beitz AJ. Nociceptive characteristics of tumor necrosis factor-alpha in naive and tumor-bearing mice. Neuroscience. 2005; 132(2):479–491. [PubMed: 15802198]
70. Wagner R, Myers RR. Endoneurial injection of TNF-alpha produces neuropathic pain behaviors. Neuroreport. 1996; 7(18):2897–2901. [PubMed: 9116205]
71. Wagner R, Myers RR. Schwann cells produce tumor necrosis factor alpha: expression in injured and non-injured nerves. Neuroscience. 1996; 73(3):625–629. [PubMed: 8809782]
72. Watanabe H, Iwase M, Ohashi M, Nagumo M. Role of interleukin-8 secreted from human oral squamous cell carcinoma cell lines. Oral Oncol. 2002; 38(7):670–679. [PubMed: 12167419]
73. Waxman SG, Zamponi GW. Regulating excitability of peripheral afferents: emerging ion channel targets. Nat Neurosci. 2014; 17(2):153–163. [PubMed: 24473263]
74. Woolf CJ, Allchorne A, Safieh-Garabedian B, Poole S. Cytokines, nerve growth factor and inflammatory hyperalgesia: the contribution of tumour necrosis factor alpha. Br J Pharmacol. 1997; 121(3):417–424. [PubMed: 9179382]
75. Ye Y, Dang D, Zhang J, Viet CT, Lam DK, Dolan JC, Gibbs JL, Schmidt BL. Nerve growth factor links oral cancer progression, pain, and cachexia. Molecular cancer therapeutics. 2011; 10(9): 1667–1676. [PubMed: 21750223]
76. Ye Y, Ono K, Bernabe DG, Viet CT, Pickering V, Dolan JC, Hardt M, Ford AP, Schmidt BL. Adenosine triphosphate drives head and neck cancer pain through P2X2/3 heterotrimers. Acta neuropathologica communications. 2014; 2:62. [PubMed: 24903857]
77. Yuan B, Hu LH, Lentsch EM, Shum-Siu A, Hendler FJ. Consistent allelic loss on mouse chromosome 7 distal to tyrosinase in 4-nitroquinoline-1-oxide-induced oral cavity tumors with loss of heterozygosity at Ha-ras-1. Mol Carcinog. 1997; 19(1):8–16. [PubMed: 9180923]
78. Yuan B, Oechsli MN, Hendler FJ. A region within murine chromosome 7F4, syntenic to the human 11q13 amplicon, is frequently amplified in 4NQO-induced oral cavity tumors. Oncogene. 1997; 15(10):1161–1170. [PubMed: 9294609]
79. Zandberg DP, Strome SE. The role of the PD-L1:PD-1 pathway in squamous cell carcinoma of the head and neck. Oral Oncol. 2014; 50(7):627–632. [PubMed: 24819861]
80. Zhao X, Rong L, Zhao X, Li X, Liu X, Deng J, Wu H, Xu X, Erben U, Wu P, Syrbe U, Sieper J, Qin Z. TNF signaling drives myeloid-derived suppressor cell accumulation. J Clin Invest. 2012; 122(11):4094–4104. [PubMed: 23064360]

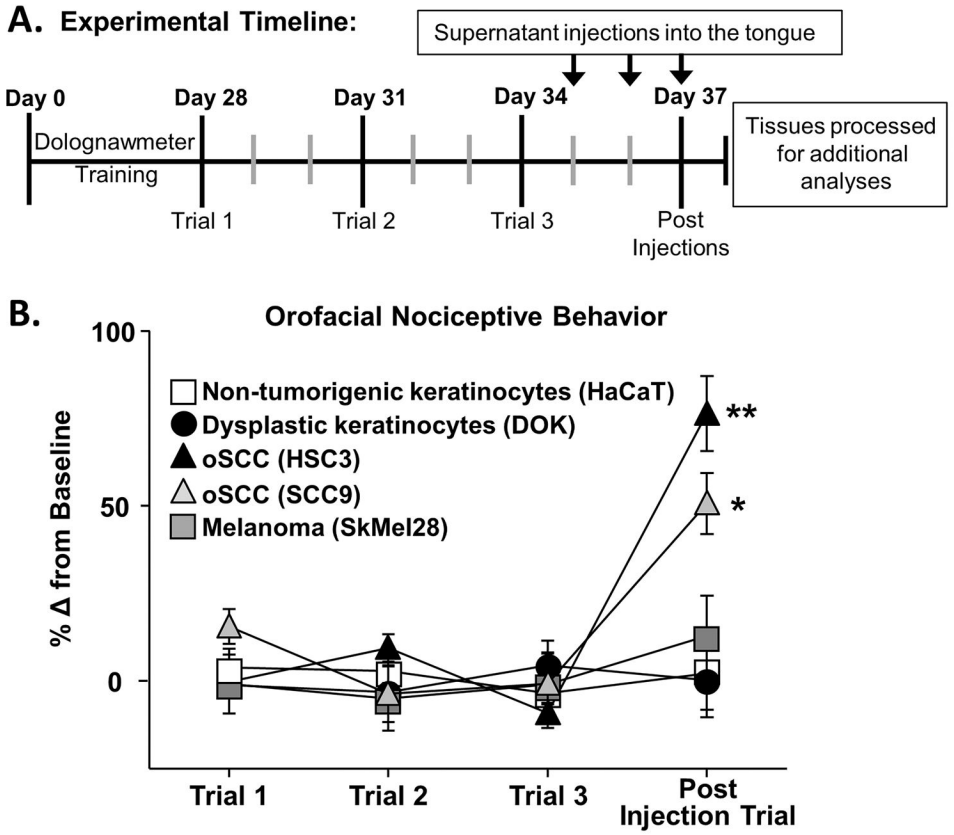

Figure 1. Oral cancer-secreted mediators evoked orofacial nociceptive behavior

A) Schematic of the experimental timeline for an acute cell line supernatant model of oral cancer pain. Adult C57BL/6 female mice were trained for 4 weeks in the orofacial pain behavior device and assay (dolognawmeter) or until a steady baseline was reached. Three additional baseline trials were completed and then mice underwent 3 consecutive injections of cell line supernatant followed by assessment in the dolognawmeter (Post Injection Trial). Twelve hours after the last injection, tissues were processed for additional analysis. There was no change in gnaw time between groups; therefore, 3 baseline trials for each group were averaged and analyzed as a percent change. Pooled data (**B**) indicate that only oral cancer cell lines supernatant, HSC3 (black triangle, n = 15) and SCC9 (gray triangle, n = 9), injections evoked a significant increase in gnaw time compared to an immortalized non-tumorigenic keratinocyte cell line (HaCaT, white square, n = 10), precancerous dysplastic oral keratinocytes (DOK, black circle, n = 9), and clinically non-painful cancer, skin melanoma (SkMel28, gray square, n = 9). Data are represented as a percent change from the average baseline trials (Paired Student's *t* test, * $p < 0.05$, ** $p < 0.01$).

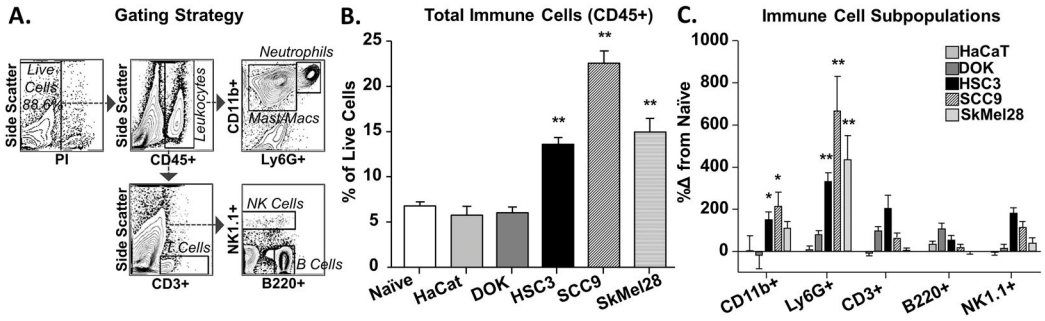

Figure 2. Cancer-secreted mediators recruited immune cells to the tongue microenvironment

Tongue tissue from naïve mice (n = 9) and mice after 3 consecutive injections of cell line supernatant from HaCaT (n = 10), DOK (n = 6), HSC3 (n = 10), SCC9 (n = 10), and SkMel28 (n = 6) were analyzed using flow cytometry. **A**) Representative gating strategy used to isolate immune cell subpopulations from a mouse tongue treated with HSC3 supernatant. CD45+ immune cells were isolated first from the population of live cells as determined by vitality marker, propidium iodide (PI), and then sorted into macrophages/monocytes/neutrophils (CD11b+) and dendritic cells (CD11c+) (not shown) or sorted into T cells (CD3+). The CD11b+ cells were further sorted into macrophages/monocytes (CD11b+Ly6G−) and neutrophils (CD11b+Ly6G+). The CD3− cells were further sorted into natural killer (NK) cells (NK1.1+) or B cells (B220+). All pooled data are expressed as a percent of total live cells. One-way ANOVA analysis of pooled CD45+ cells (**B**) indicated a significant difference between oral cancer cell line supernatant (HSC3, SCC9) treatment and naïve tongues (* $p < 0.05$, ** $p < 0.01$). **C**) Further gating of CD45+ cells into immune cell subpopulations identified significantly increased neutrophils (Ly6G+) and macrophages/monocytes (CD11b+) in the tongue tissue in response to HSC3 and SCC9 (One-way ANOVA, * $p < 0.05$, ** $p < 0.01$). There was no change in T cells (CD3+), B cells (B220+) or NK cells (NK1.1) subpopulations in response to any cell line supernatant compared to naïve tongue tissue (One-way ANOVA, $p > 0.05$).

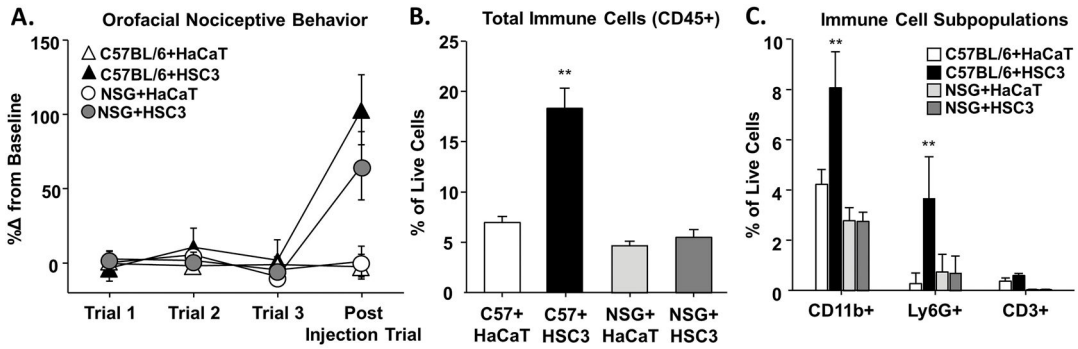

Figure 3. Oral cancer-secreted mediators evoked orofacial nociceptive behavior in immune-deficient mice

The cell line supernatant model of oral cancer pain was used to measure nociceptive behavior in response to cell line supernatant in immune-deficient (NSG) mice compared to immune-competent (C57BL/6) mice. Pooled data (**A**) indicate that HSC3 supernatant evoked a significant increase in gnaw time in C57BL/6 (black triangle, n = 5) and NSG (gray circle, n = 5) mice compared to HaCaT supernatant (white triangles and circle, n = 5). Flow cytometry on the tongue tissue from these mice was used to measure the inflammatory infiltrate. **B)** In C57BL/6 mice only, HSC3 injection resulted in a significant increase in the percent of CD45+ immune cells in the tongue compared HaCaT supernatant (One-way ANOVA, ** $p < 0.01$). Analysis of CD45+ immune cell subpopulations (**C**) indicated a significant increase in the macrophages/monocytes (CD11b+) and neutrophils (Ly6G+) subpopulations in response to HSC3 supernatant (One-way ANOVA, ** $p < 0.01$) but no change in infiltrating T cells (CD3+).

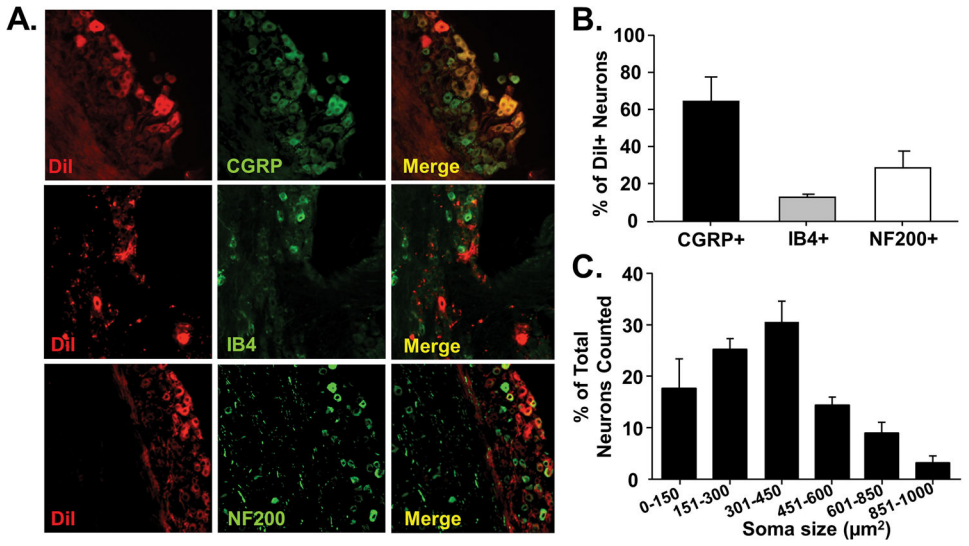

Figure 4. Predominantly peptidergic primary afferent neurons innervate the tongue

Tongue afferent neuron labeling using the lipophilic retrograde tracer, DiI. **A)** Representative images from co-staining of DiI-positive (red) TG sections with CGRP (top, green), IB4-FITC (middle, green), and NF200 (bottom, green). Co-expression is indicated by yellow overlap (Merge). **B)** Pooled data from 3 female TG pairs indicated that DiI-positive neurons had predominantly more CGRP-immunolike reactivity (IR) (64.3 ± 13.2%) compared to IB4-IR (13.2 ± 1.6%) and NF200-IR (29 ± 8.9%) populations. **C)** Histogram of neuronal size distribution of cells retrogradely labeled from the tongue. Tongue afferent neurons are predominately small to medium (soma size 151–450 μm^2).

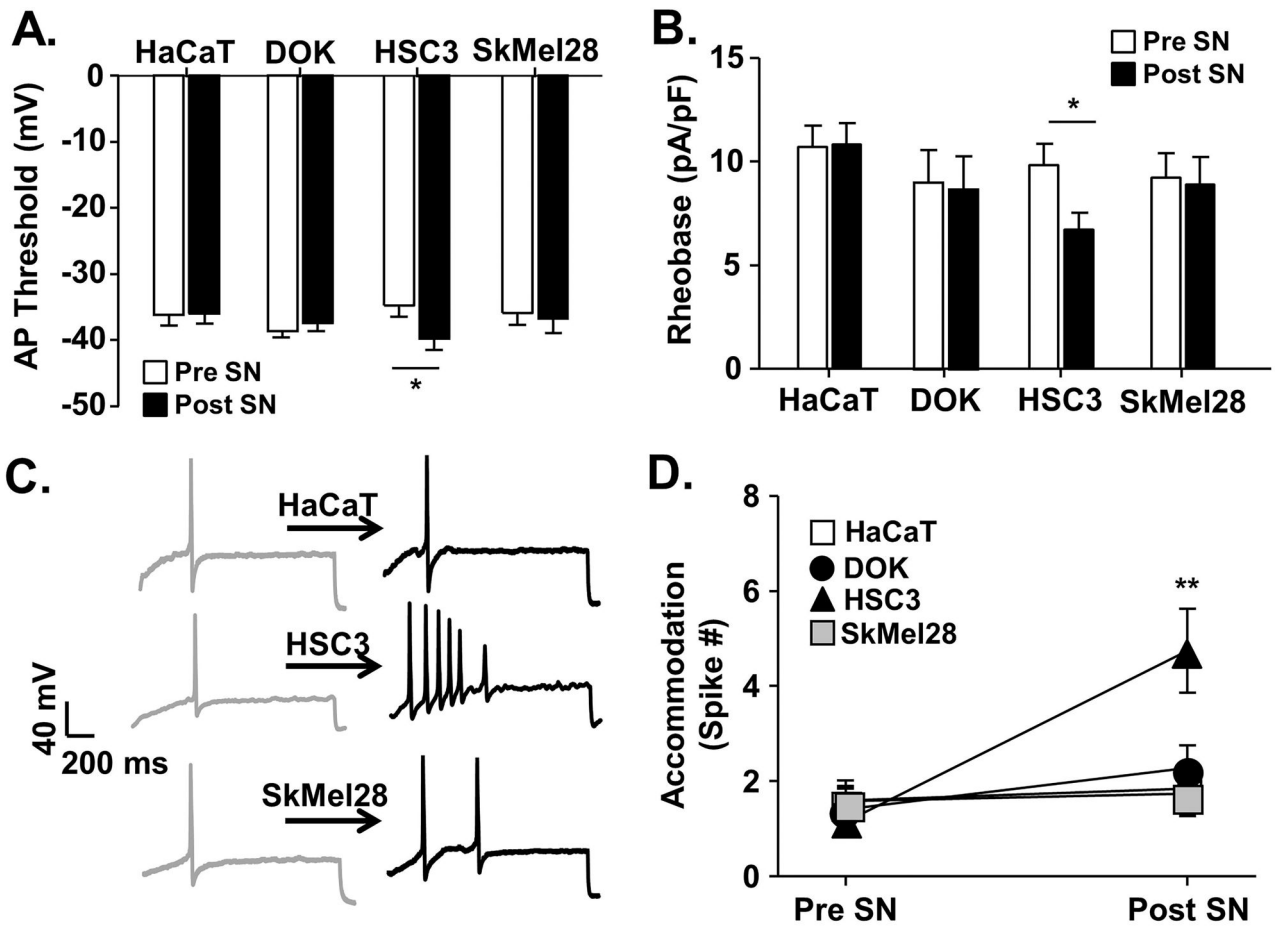

Figure 5. Oral cancer-secreted mediators induced neuronal excitability

Whole cell current clamp electrophysiology was used to measure primary afferent neuron excitability following acute application of cell line supernatant. Application of HSC3 resulted in an increase in excitability parameters in retrogradely labeled (DiI+) dissociated trigeminal ganglia neurons (n = 5 mice, 24 neurons), whereas cell line supernatant from non-tumorigenic keratinocytes (HaCat, n = 4 mice, 19 neurons), precancerous dysplastic keratinocytes (DOK, n = 4 mice, 17 neurons), and melanoma (SkMel28, n = 4 mice, 12 neurons) did not. Data **(A–C)** assessed before (Pre SN) and after (Post SN) cell line supernatant application to tongue afferent neurons were pooled and plotted as means ± SE. There was a significant HSC3-induced decrease in rheobase (**A**) and AP threshold (**B).** Representative traces (**C**) illustrate action potentials evoked with a 250 millisecond ramp followed by a 500 millisecond sustained current injection protocol (accommodation) in single neurons at baseline and in response to cell line supernatant. Pooled data (**D**) demonstrate a significant increase in the number of spikes evoked after application of oral cancer cell line supernatant only. There was no difference in baseline excitability prior to cell line supernatant application; therefore, data was analyzed as a percent change from baseline using One-way ANOVA (* $p < 0.05$, ** $p < 0.01$).

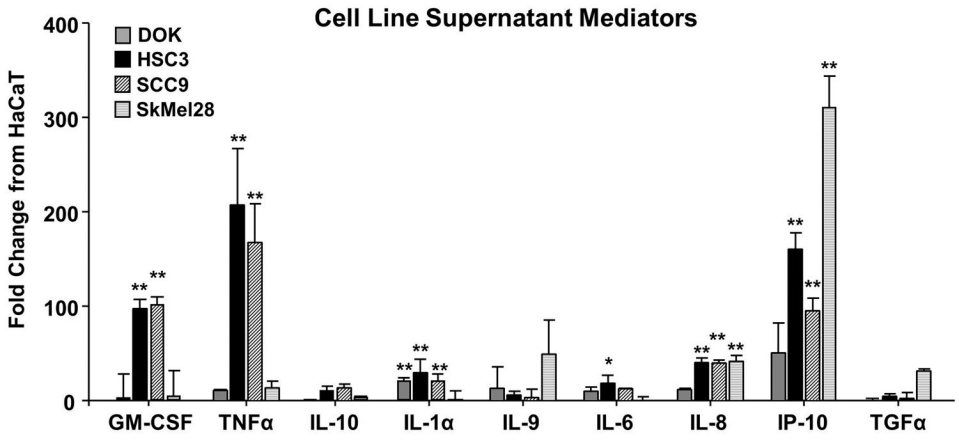

Figure 6. Analysis of cell line supernatant protein contents revealed multiple pro-inflammatory and pro-nociceptive mediators

Cytokines present in supernatants of cancer cell lines (HSC3, SCC9) as well as precancerous dysplastic oral keratinocytes (DOK) cell line, melanoma (SkMel28) cell line, and immortalized non-tumorigenic keratinocytes (HaCaT) cell line were quantitated using MILLIPLEX® MAPmultiplex cytokine biomarker magnetic bead panel for detection of 38 mouse cytokines and chemokines. Pooled data demonstrate that of the 38 mediators measured, 9 had a ≥ 10-fold change in DOK (gray), HSC3 (black), SCC9 (black stripe), or SkMel28 (gray stripe) compared to HaCaT. Two-way ANOVA demonstrated a significant interaction between cell lines tested and mediators measured ($p < 0.01$). Dunnett's post hoc analysis is represented on the graph (* $p < 0.05$, ** $p < 0.01$).

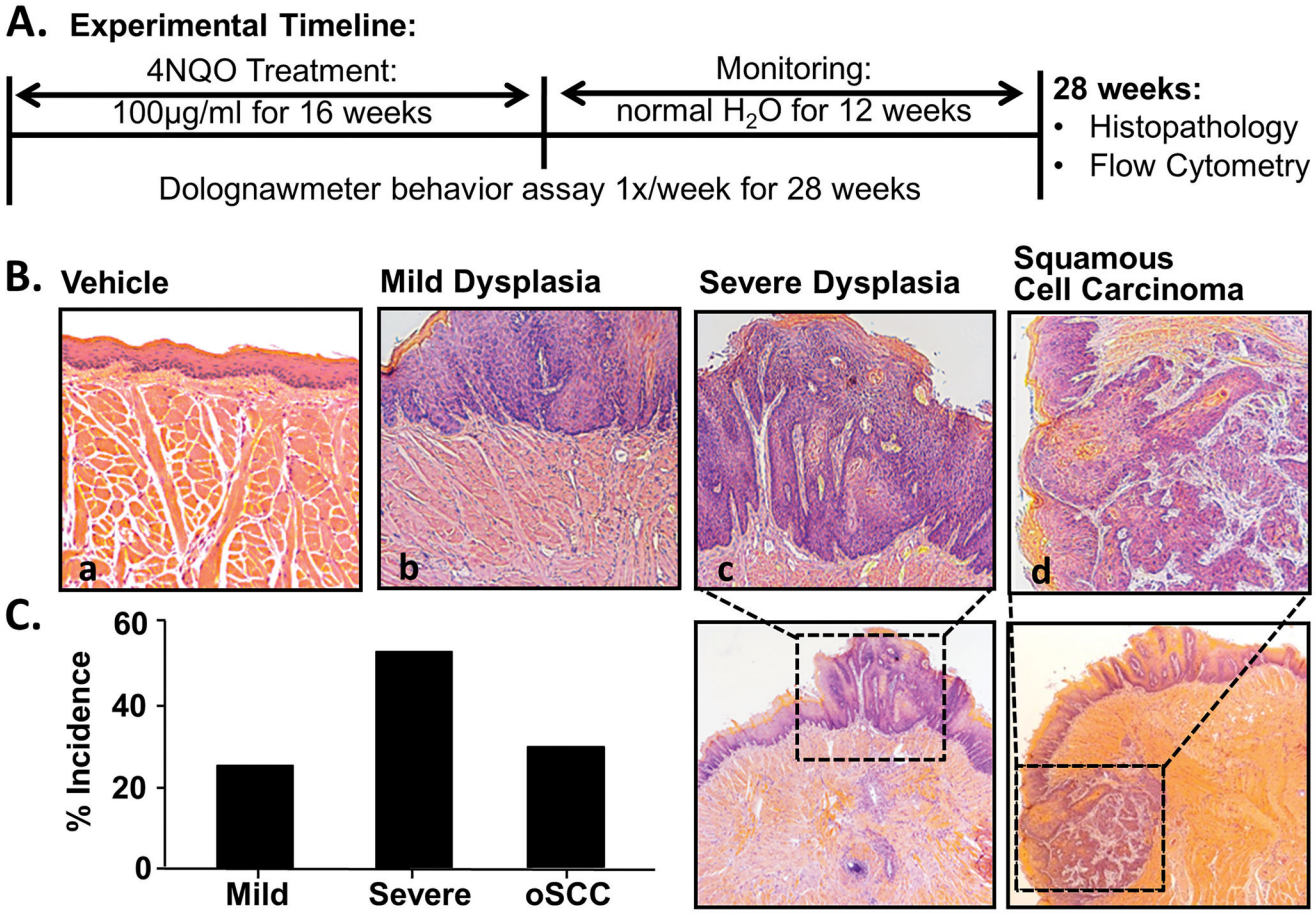

Figure 7. 4NQO-induced mouse model of oral squamous cell carcinoma

A) Schematic of the experimental design during which a total of 45 mice received either 100 µg/mL 4NQO or propylene glycol (vehicle) in the drinking water *ad lib* for 16 weeks followed by an additional 12 week monitoring period (normal water). During this time, mice underwent dolognawmeter assay 1× per week for the full 28 weeks to measure functional allodynia during carcinogenesis. At the completion of the study, tongue tissue was processed for histopathology and flow cytometry. **B**) Representative hematoxylin & eosin stained histological tongue sections from a vehicle-treated mouse (**a**; 20×) and 4NQO-treated mice with mild dysplasia (**b**; 20×), severe dysplasia (**c;** 10× with 20× inset), and invasive carcinoma (**d;** 10× with 20× inset). 4NQO treatment resulted in lesions within the oral cavity. Pooled data demonstrated the percent incidence of the stages of carcinogenesis.

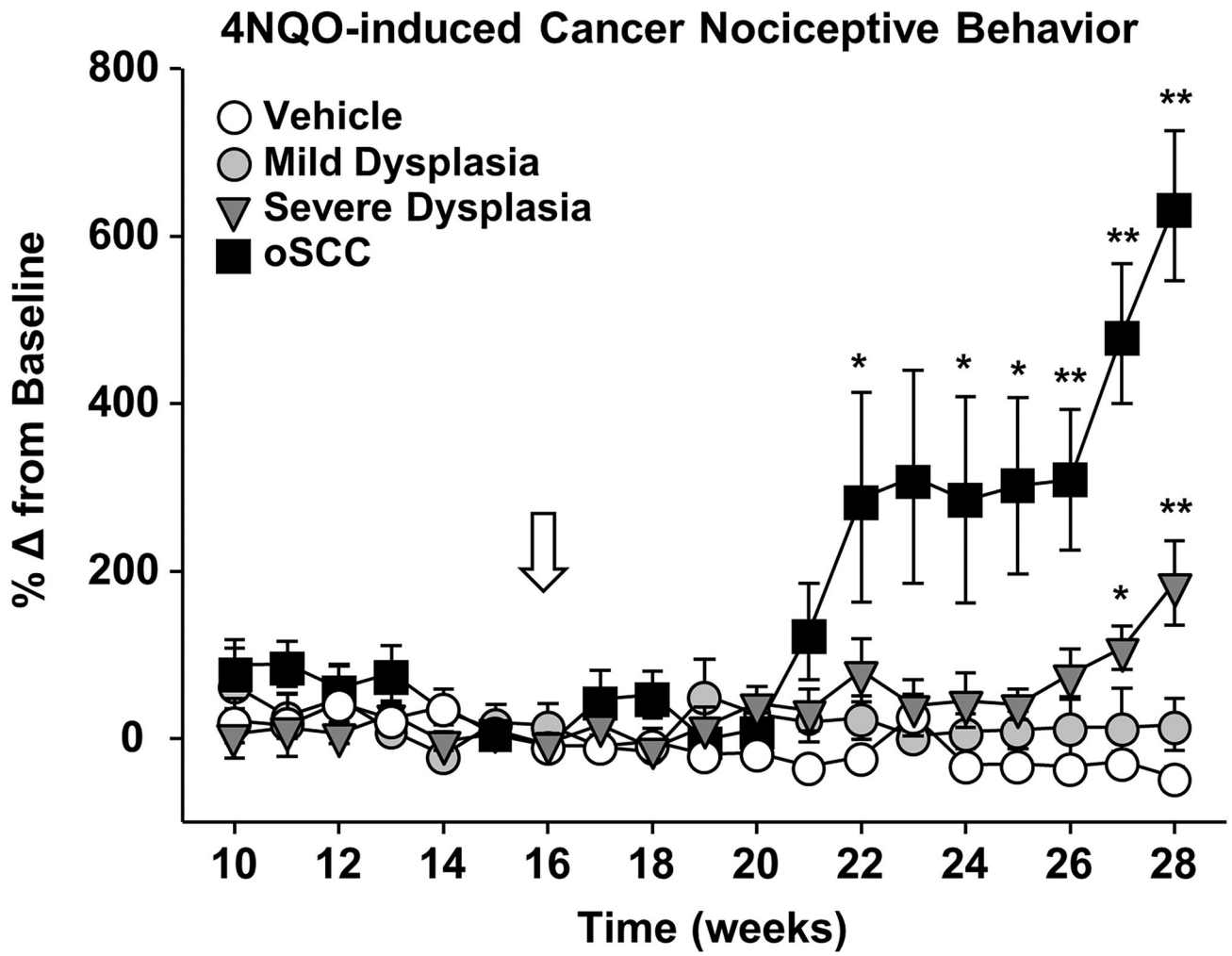

Figure 8. 4NQO-induced squamous cell carcinoma development evoked chronic functional allodynia

Mice developed oral squamous cell carcinoma (oSCC) following 4NQO exposure for 16 weeks (white arrow). Mice were classified by the tongue histopathology: mild dysplasia (black circles, n = 7), severe dysplasia (black triangle n = 16), or oSCC (black squares, n = 12) compared to vehicle-treated mice (white circle, n = 10). Functional allodynia was analyzed as mean gnaw time across mice with similar histopathology over time (weeks). Two-way ANOVA analyses of pooled data from mice with mild dysplasia, severe dysplasia and oSCC over time indicated a significant interaction between carcinogenesis and time for both mice with severe dysplasia ($p < 0.01$) and oSCC ($p < 0.01$). Holm-Sidak post hoc comparisons reveal significant differences between mice with severe dysplasia and oSCC during the last 6 weeks of the study (* $p < 0.05$, ** $p < 0.01$).

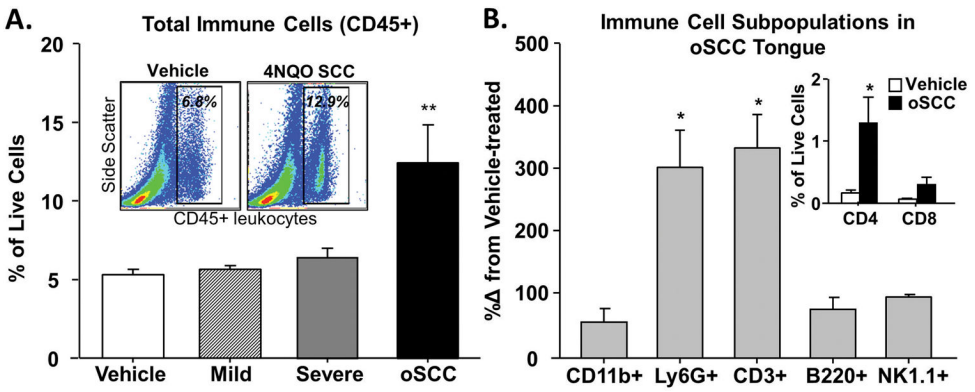

Figure 9. Increased immune cell infiltrate during the development of 4NQO-induced oSCC

Using flow cytometry, infiltrating immune cells were quantified in dissociated tongue tissue from vehicle-treated (white bars), 4NQO-induced mild (striped bars) and severe (gray bars) dysplasia, and oSCC (black bars) mice. **A**) One-way ANOVA analysis of pooled data, expressed as a percent of total live cells, revealed significant differences in total immune cells (CD45+) in the tongue during carcinogenesis compared to vehicle-treated mice (indicated by ** $p < 0.01$). Representative contour plots of cells quantified from vehicle-treated and 4NQO-treated oSCC mice demonstrate the significant increase in CD45+ cells (**A, Inset**). Further analysis in tissue from 4NQO-treated mice with oSCC (**B**) revealed a significant increase in T cells (CD3+) and neutrophils (Ly6G+) (One-way ANOVA, * $p < 0.05$, ** $p < 0.01$); data are presented as a percent change from tongues of vehicle-treated mice. There was no significant change in B cells (B220+) or NK cells (NK1.1+). Subsequent sorting revealed that T helper cells (CD3+CD4+) and cytotoxic T cells (CD3+CD8+) are increased in oSCC tongue tissue compared to vehicle-treated tongue tissue (**B, Inset**).

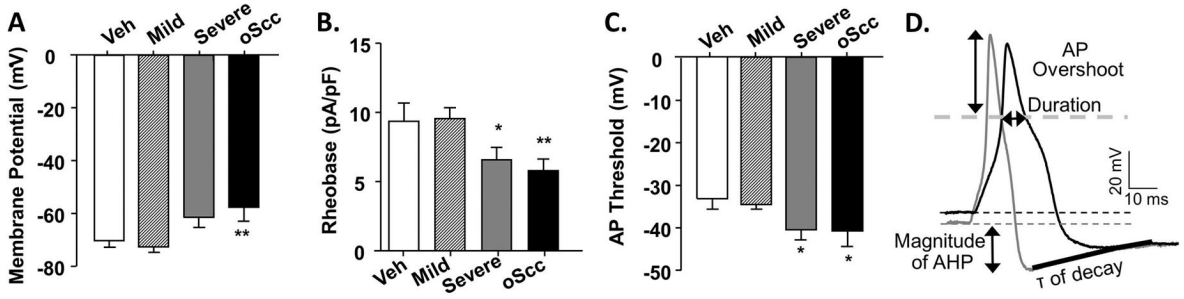

Figure 10. Neuronal sensitization during the progression of 4NQO-induced oral carcinogenesis

Excitability was quantified with resting membrane potential **(A),** rheobase **(B),** and action potential (AP) threshold **(C)** in TG neurons from vehicle-treated mice (white bars, n = 5) and 4NQO-treated mice. Excitability parameters were analyzed across mice with similar histopathology: mild dysplasia (striped bars, n = 6) and severe (gray bars, n = 4) dysplasia, and oSCC (black bars, n = 5). One-way ANOVA analysis revealed significant differences between the 3 stages of cancer progression compared to neurons from vehicle-treated mice. Holm-Sidak post-hoc analysis showed significant differences between groups (as indicated, * $p < 0.05$, ** $p < 0.01$). **D)** A representative depolarization (4 milliseconds) evoked AP from a vehicle-treated (gray) and 4NQO-treated mouse with oSCC (black) in which we defined the active electrophysiological properties analyzed in Table 2. **τ** is time constant of AHP decay.

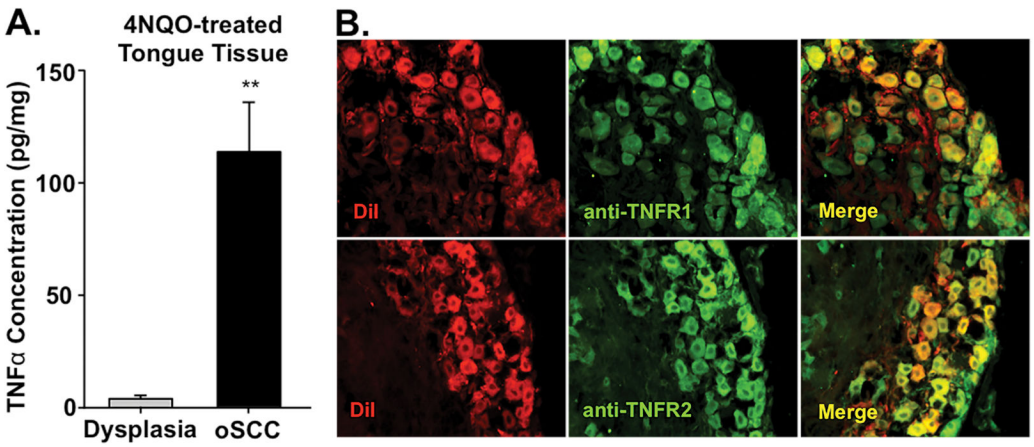

Figure 11. 4NQO-induced changes in TNFα protein in tongue microenvironment and associated receptors in tongue afferent neurons

Tongue tissue from 4NQO-treated and vehicle-treated mice was homogenized and TNFα protein was measured using an ELISA kit. A) The TNFα concentration (pg/mg) was significantly increased in oSCC tongue tissue (n = 6) compared to mild dysplasia tongue tissue (n = 5). TNFα concentrations were normalized to total protein concentration (pg/mL) in the sample. TNFα protein in vehicle-treated tongues was below the level of detection. B) Representative 20× images of TG neuron sections retrogradely labeled with DiI (red) and immunostained for TNFα receptor 1 and 2 (green). Overlap of DiI and TNF receptors immunolike reactivity is indicated in yellow.

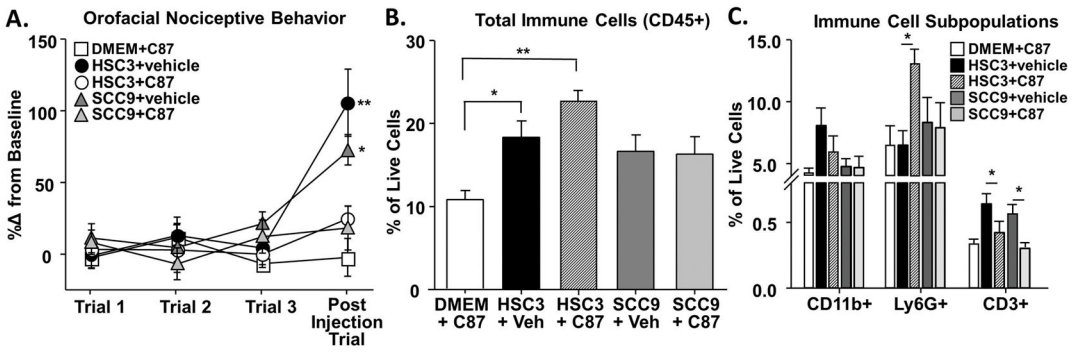

Figure 12. Removing TNFα from oral cancer cell line supernatant abolished functional allodynia

TNFα inhibitor (C87) was used to inhibit TNFα signaling in the presence of oral cancer cell line supernatant. We used the acute cell line supernatant model described in Figure 1 during which mice received 3 consecutive injections of either oral cancer cell line supernatant, HSC3 or SCC9, alone or in a co-injection with C87. Pooled data (**B**) indicate that C87 alone (C87+DMEM, white square) does not affect gnawing behavior. However, HSC3 (black circle) and SCC9 (gray triangle) containing 0.02% DMSO (HSC3+vehicle and SCC9+vehicle, respectively) evoked a significant increase in gnaw time. Co-administration of C87 with HSC3 (HSC3+C87, white circle, n = 5) or SCC9 (SCC9+C87, white triangle, n = 5) abolished the oral cancer cell line supernatant-induced pain behavior. Flow cytometry on the tongue tissue from these mice was used to measure the inflammatory infiltrate. **B)** C87+DMEM had no effect on the percent of CD45+ immune cells in the tongue compared to oral cancer cell line supernatant alone (HSC3+veh, SCC9+veh). However, within the Cd45+ immune cell subpopulations **(C)** there was a significant increase in the neutrophils (Ly6G+) in response to HSC3+C87 co-injection compared to HSC3+vehicle. Co-injection of C87 with either HSC3 or SCC9 also resulted in a significant decrease in T cells (CD3+) compared to HSC3+vehicle or SCC9+vehicle respectively (One-way ANOVA, * $p<0.05$).

Table 1

Cell line supernatant-evoked changes in passive properties of evoked action potentials from tongue afferents expressed as % change from baseline.

		Average Capacitance (pf)	%Δ Membrane Potential (mV)	%Δ Input Resistance (mω)
HaCat	(n=18)	14.3 ± 3.3	3.8 ± 1.8	−2.3 ± 12.9
DOK	(n=13)	12.5 ± 4.6	2.7 ± 6.3	−25.81 ± 10.7
HSC3	(n=24)	13.7 ± 3.9	−16.9 ± 2.8 **	−51.5 ± 9.7 **
SkMel28	(n=13)	14.4 ± 2.9	3.7 ± 1.4	1.23 ± 10.4

Table 2

Passive and active parameters of the evoked action potential from tongue afferents from female mice studied as vehicle treated, and 4NQO-induced mild dysplasia, severe dysplasia and oSCC.

	# of neurons	Capacitance (pf)	Input Resistance (mω)	Overshoot (mV)	Duration (ms)	AHP Magnitude (mV)	τ of decay (ms)
Vehicle	(n=21)	12.2 ± 1.1	1704.6 ± 212.8	61.4 ± 1.8	3.2 ± 0.3	−15.2 ± 0.9	61.7 ± 17.7
Mild Dysplasia	(n=36)	15.5 ± 5.7	1541.1 ± 594.8	64.6 ± 7.9	2.8 ± 0.4	13.6 ± 0.9	85.6 ± 21.2
Severe Dysplasia	(n=24)	14.3 ± 4.6	1576.8 ± 935.8	55.9 ± 4.8	3.9 ± 1.7	−18.1 ± 3.1	101.6 ± 12.1
oSCC	(n=18)	14.2 ± 4.6	1389.3 ± 361.0	42.6 ± 3.6*	2.6 ± 0.2	−15.5 ± 1.1	127.6 ± 16.8*